Environmental Science and Ecotechnology 22 (2024) 100469

Contents lists available at ScienceDirect

Environmental Science and Ecotechnology

journal homepage: www.journals.elsevier.com/environmental-science-and-ecotechnology/

Review

Applying molecular oxygen for organic pollutant degradation: Strategies, mechanisms, and perspectives

Xiaohu Fan [a, b], Qiang Fu [a, b], Guorui Liu [c], Hongliang Jia [d], Xiaolong Dong [a, b], Yi-Fan Li [a, b], Song Cui [a, b, *]

[a] International Joint Research Center for Persistent Toxic Substances (IJRC-PTS), School of Water Conservancy and Civil Engineering, Northeast Agricultural University, Harbin, 150030, China
[b] Research Center for Eco-Environment Protection of Songhua River Basin, Northeast Agricultural University, Harbin, 150030, China
[c] State Key Laboratory of Environmental Chemistry and Ecotoxicology, Research Center for Eco-Environmental Sciences, Chinese Academy of Sciences, Beijing, 100085, China
[d] IJRC-PTS, College of Environmental Science and Engineering, Dalian Maritime University, Dalian, 116026, China

ARTICLE INFO

Article history:
Received 22 February 2024
Received in revised form
26 July 2024
Accepted 29 July 2024

Keywords:
Reactive oxygen species
Activation strategies
Molecular oxygen
Organic pollutant degradation

ABSTRACT

Molecular oxygen (O_2) is an environmentally friendly, cost-effective, and non-toxic oxidant. Activation of O_2 generates various highly oxidative reactive oxygen species (ROS), which efficiently degrade pollutants with minimal environmental impact. Despite extensive research on the application of O_2 activation in environmental remediation, a comprehensive review addressing this topic is currently lacking. This review provides an informative overview of recent advancements in O_2 activation, focusing on three primary strategies: photocatalytic activation, chemical activation, and electrochemical activation of O_2. We elucidate the respective mechanisms of these activation methods and discuss their advantages and disadvantages. Additionally, we thoroughly analyze the influence of oxygen supply, reactive temperature, and pH on the O_2 activation process. From electron transfer and energy transfer perspectives, we explore the pathways for ROS generation during O_2 activation. Finally, we address the challenges faced by researchers in this field and discuss future prospects for utilizing O_2 activation in pollution control applications. This detailed analysis enhances our understanding and provides valuable insights for the practical implementation of organic pollutant degradation.

1. Introduction

The rapid advancement of industrial civilization has led to the proliferation of various organic contaminants, including antibiotics [1], pesticides [2], personal care products [3], and surfactants [4]. These substances pose significant threats to ecological systems and human health due to their high toxicity and extensive production. Their inherent structural stability makes them resistant to natural degradation processes [5]. Advanced oxidation processes (AOPs) have gained widespread recognition for their efficacy in degrading organic pollutants [6,7]. AOPs facilitate the abundant generation of reactive oxygen species (ROS) by harnessing the potential of highly reactive oxidants within optimal catalytic environments. These potent agents play a pivotal role in decomposing a wide range of organic pollutants, encompassing organic compounds in industrial wastewater [8], agricultural pollutants [9], and pharmaceutical residues in medical wastewater [10]. The strategic implementation of AOPs is crucial for improving water quality, preserving the ecological environment, and promoting sustainable development principles.

At present, AOPs encompass a variety of methodologies, including Fenton and Fenton-like processes [11], photocatalytic methods [12], and electrocatalytic techniques [13]. The ROS generated by these modalities possess distinct attributes that influence their effectiveness in contaminant removal. These ROS are produced through redox reactions. Traditionally, the majority of ROS are produced through electron acquisition. However, the pathway's sources for electron donors are diverse, primarily including metals, oxidants, photonic energy, and electric currents.

* Corresponding author. International Joint Research Center for Persistent Toxic Substances (IJRC-PTS), School of Water Conservancy and Civil Engineering, Northeast Agricultural University, Harbin, 150030, China.
E-mail address: cuisong-bq@neau.edu.cn (S. Cui).

https://doi.org/10.1016/j.ese.2024.100469

For example, the classical Fenton reaction represents a reduction pathway for generating hydroxyl radicals (•OH), where Fe^{2+} acts as an electron donor to produce hydrogen peroxide (H_2O_2), resulting in •OH and Fe^{3+}. Photo-generated electrons can activate peroxymonosulfate (PMS), leading to the production of •OH and $•SO_4^-$ [14]. Additionally, PMS can acquire electrons from low-valence metals to generate •OH [15]. On the other hand, oxidation reactions also play a crucial role in ROS generation. High-value metals can directly oxidize prevalent oxidants into various ROS [16]. For example, Mn^{3+} can directly oxidize PMS and H_2O_2 to yield superoxide radicals ($•O_2^-$) [17]. Mo^{6+} possesses the ability to transform $•O_2^-$ into singlet oxygen ($^1O_2$) [18]. Within the photocatalytic process, the oxidation of $•O_2^-$ by photoinduced holes represents one avenue for producing $^1O_2$ [19]. Additionally, water oxidation is widely recognized as a precursor to ROS. Tungsten trioxide and zinc sulfide possess abundant valence band holes, facilitating the direct oxidation of hydroxide ions (OH^-) or water molecules to generate •OH, which actively participates in the decomposition of tetracycline (TC) [20]. Various AOPs currently exist that can generate a significant amount of ROS, thereby aiding in eliminating pollutants. While these conventional methodologies have demonstrated their effectiveness, they often pose risks of causing secondary pollution. Therefore, there is an urgent need to explore novel technologies capable of efficiently degrading environmental contaminants.

Molecular oxygen (O_2), acclaimed for its environmental friendliness and cost-efficiency, is ubiquitously accessible in the atmosphere. However, the direct oxidation of numerous organic contaminants by O_2 is hindered due to spin-forbidden reactions [21]. In contrast, the activation of O_2 can generate various ROS, including $•O_2^-$, $^1O_2$, •OH, and H_2O_2. These ROS play a pivotal role as oxidizing agents in the decomposition processes of organic compounds.

Given the significance of activating O_2, this review provides a comprehensive analysis of research advancements in the degradation of organic contaminants through the activation of O_2. This paper extensively discusses primary strategies for activating O_2 to degrade organic molecules, including photocatalytic, chemical, and electrochemical methods. Moreover, it intricately dissects factors influencing O_2 activation and explores generative pathways of ROS considering electron transfer and energy transfer dimensions. This concludes with a discussion of prospects for novel degradation approaches through O_2 activation. This article aims to enhance understanding of O_2 activation methodologies and their role in environmentally removing organic pollutants.

2. Photocatalytic oxygen activation

The degradation of organic pollutants via the photochemical activation of O_2 involves the conversion of dissolved O_2 into various ROS. Based on the generation of ROS, this conversion mechanism can occur via two principal pathways: energy transfer or electron transfer [22]. The efficiency of ROS generation in this innovative oxidation process depends on several factors, including the performance characteristics of the semiconductor, the illumination mode, and the source of O_2.

2.1. Metal-based photocatalysts

Recently, various metal oxides, including titanium dioxide (TiO_2), zinc oxide (ZnO), copper(I) oxide (Cu_2O), and iron oxide (Fe_2O_3), have been applied to activate oxygen for the degradation of organic pollutants under light irradiation. Notably, bismuth-containing photocatalysts have emerged as crucial semiconductors in this field.

Zhao et al. [23] employed a solvent-thermal modification technique to synthesize BiOCl, wherein the exposure to a 300 W xenon lamp activated O_2, resulting in the prolific generation of $•O_2^-$ and $^1O_2$. With a modest quantity of H_2O_2, the rhodamine B (RhB), methyl orange (Mo), and phenol decomposition rates were amplified by 2.6, 3.1, and 2.4 times, respectively. $^1O_2$ is generated as a result of the energy transfer or electron transfer. Wang et al. [24] ingeniously crafted an iodine-doped Bi_2WO_6 catalyst that created high-density oxygen vacancies (OVs) to enhance the photochemical activation of O_2. Their findings indicated that $•O_2^-$ and $^1O_2$ were the principal ROS implicated in the disintegration of sodium pentachlorophenate (NaPCP) [24]. Nd-doped BiO_{2-x} exhibited proficient near-infrared ray light-driven photocatalytic O_2 activation, where the abundant production of $•O_2^-$ accelerated doxycycline degradation with a reaction rate constant reaching up to 134.4×10^{-4} min^{-1} [25]. In the photochemical activation process, two-electron reduction of O_2 is the main pathway for H_2O_2 formation, which is an important ROS in pollutant degradation [25]. Sheng et al. [26] investigated the photocatalytic prowess of Bi_2WO_6 under visible light irradiation using phenol as a prototypical pollutant. Their findings revealed that post-irradiation treatment resulted in the liberation of photo-induced electrons from Bi_2WO_6 capable of converting O_2 into H_2O_2. In the presence of electrons, H_2O_2 undergoes decomposition to yield the highly oxidative •OH, thereby accelerating the efficient degradation of phenol. Liu et al. [27] engineered an iodine-doped Bi_2MoO_6 semiconductor and developed a light-stimulated H_2O_2 production system. This system demonstrated a 96.0% efficiency in the photodegradation of acetaminophen (APAP).

In addition to Bi-based photocatalysts, iron oxides have also been frequently mentioned for their effectiveness in the photocatalytic activation of O_2. Yue et al. [28] reported synthesizing a Z-type heterojunction 0Dα-Fe_2O_3/TiO_2. The Z-scheme charge transfer mechanism significantly accelerated the Fe^{3+}/Fe^{2+} cycling rate, optimizing the utilization of H_2O_2 for •OH generation. This system demonstrated superior degradation efficacy against 2,4-dichlorophenol (2,4-DCP), achieving a degradation kinetic rate constant of 1.08 min^{-1}. Another advanced photocatalyst, N-GQDs/$Bi_2Fe_4O_9$, was designed to oxidize organic contaminants [29]. Upon light exposure, N-GQDs/$Bi_2Fe_4O_9$ exhibited remarkable H_2O_2 production (1.6 μM min^{-1}). Moreover, electrons congregating around N-GQDs enhanced the redox cycling of Fe^{3+}/Fe^{2+} reactions, promoting •OH production and resulting in a 99.9% bisphenol A (BPA) elimination rate.

Metal sulfides, characterized by their narrow band gap, exhibit remarkable responsiveness to visible light and have thus been utilized in synthesizing photocatalysts for degrading organic pollutants by activating O_2 [30]. In scenarios where the ROS generated through photocatalytic O_2 activation is H_2O_2, this process is also called the photo-Fenton system [31]. Yang et al. [32] designed a CdS/Fe^{2+} photo-Fenton system to degrade sulfamethazine (SMT) under visible light, highlighting the capability of CdS nanorods in converting O_2 to H_2O_2 via a direct two-electron reduction pathway. Similarly, Jiang et al. [33] developed a CdS/rGO/Fe^{2+} photo-Fenton system capable of degrading phenol through *in situ* H_2O_2 generation under visible light irradiation. Their findings suggested that the *in situ* production of H_2O_2 in this system may follow a two-electron, one-step reduction mechanism.

The photo-Fenton process, which involves the reduction of dissolved O_2 under light irradiation, is regarded as an innovative strategy. Shi et al. [34] developed a CdS/reduced graphene (rGO)/$ZnFe_2O_4$ (ZFO) nanocomposite system that effectively degrades TC. This degradation occurs through the *in situ* generation of H_2O_2 via a single-electron, two-step reduction of O_2 under visible light irradiation. Yang et al. [35] established a Sv-MoS_2/BN heterojunction. Upon light exposure, the Sv-MoS_2/BN-5 achieved an H_2O_2

production rate of 428.17 μmol h^{-1} g^{-1} and completed *in situ* disinfection for *Escherichia coli* (*E. coli*). Moreover, ternary metal sulfides exhibit superior catalytic activity and a broader range of properties than binary metal sulfides. Du et al. [36] synthesized $Zn_2In_2S_5$ using a meticulous *in situ* hydrothermal approach. This system can generate abundant H_2O_2 under light irradiation and exhibits excellent performance in aromatic pollutant removal, with a phenol degradation efficiency of 97.6% and an impressive H_2O_2 yield of 1.3 mmol L^{-1}. As shown in Table 1, the photocatalytic activation of O_2 has demonstrated remarkable efficiency in degrading organic pollutants through the generation of ROS.

2.2. Organic photocatalysts

The application of metal-based photocatalysts is typically hindered by their poor light responsiveness, biological toxicity, and instability [37]. In contrast, organic photocatalysts have demonstrated superior qualities such as ease of fabrication, appropriate visible light response band gap, high stability, and beneficial metal-free properties [38,39]. Currently recognized as the most prominent organic photocatalyst for activating O_2 and removing contaminants [40], graphite carbon nitride (g-C_3N_4) faces challenges due to inefficient light utilization and rapid recombination of photogenerated charge carriers that significantly impair O_2 activation [41]. To address these limitations in g-C_3N_4 photocatalytic efficiency under light irradiation, various strategies have been applied, including defect engineering [42], doping [43], the creation of ultrathin structures [44], and ion intercalation [45] (Fig. 1).

Defect engineering plays a crucial role in enhancing exciton dissociation, thereby influencing the activation of O_2. Zhou et al. [46] employed a gas reduction technique to introduce nitrogen vacancies in layered g-C_3N_4. The vacancies at the interface create a significant energy disparity, enabling the dissociation of singlet excitons into free electron-hole pairs and effectively activating O_2 to efficiently generate •OH for organic pollutant degradation. Moreover, defect engineering enhances charge separation and supports the reduction of O_2 to H_2O_2 during photocatalysis, substantially contributing to the degradation of organic pollutants. Li et al. [47] developed porous g-C_3N_4 nanosheets with carbon vacancies (Cv-PCNNS) via a two-step heat treatment approach (Fig. 1a). Their findings showed that these nanosheets exhibited remarkable capability in generating a substantial amount of H_2O_2 through a one-step dual-electron reduction reaction of O_2, achieving an impressive 984.8 μmol L^{-1} h^{-1}. Activating O_2 via photocatalysis-self-Fenton reaction achieved notable degradation efficiency for metronidazole (MTZ) (90.7%) within 100 min.

Owing to its extensive specific surface area, ultrathin material offers significant advantages in activating O_2. Hu et al. [48] synthesized a series of catalysts consisting of ultrathin g-C_3N_4 nanosheets that demonstrated high-efficiency light-driven catalytic performance in the production of H_2O_2, achieving a rate of 170.0 μmol L^{-1} h^{-1}. In the presence of this catalyst, the produced H_2O_2 can be further converted into •OH for TC degradation. Moreover, the ultrathin structure facilitates short migration distances for photo-generated carriers, enhancing O_2 reduction and H_2O_2 generation under light irradiation. Shi et al. [49] fabricated ultrathin porous g-C_3N_4 (UPCN) integrated with amorphous FeOOH quantum dots (Fig. 1b). This configuration enabled the production of 23.9 μmol L^{-1} H_2O_2 within 120 min under visible light irradiation at natural pH levels. Notably, in the photo-Fenton system, this catalyst achieved effective degradation rates of oxytetracycline (OTC) (20.0 mg L^{-1}) of 86.2% and total organic carbon (TOC) removal efficiency of 48.6% within 120.0 min.

Doping also plays a significant role in enhancing oxygen activation. Phosphorus-doped g-C_3N_4 (P-doped g-C_3N_4) has demonstrated remarkable photocatalytic reactivity in the degradation of 2,4-DCP [50] (Fig. 1c). Comparative studies have revealed that the degradation activity of 2,4-DCP can be increased by a factor of 20.5 using P-doped g-C_3N_4 compared to bulk g-C_3N_4 photocatalysis. This increase is primarily attributed to the generation of •OH from H_2O_2

Table 1
Representative studies on the degradation of organic pollutants by photocatalytic oxygen activation.

Catalysts	Mechanism	Contaminants	Reaction conditions	O_2 supply	ROS	Removal efficiency	TOC removal	Reference
OV-BOC	Energy transfer	RhB	$[RhB]_0$ = 10.0 mg L^{-1}, 300 W Xenon lamp, pH = 3.5	Dissolved oxygen	$^1O_2$, •O_2^-	99.8% (30.0 min)	-	[23]
BWO-0.18	Energy transfer	NaPCP	$[NaPCP]_0 = 30.0 \times 10^{-6}$ mg L^{-1}, 300 W Xenon lamp	Dissolved oxygen	$^1O_2$, •O_2^-	99.9% (1.0 h)	90.0%	[24]
Nd-BiO_{2-x}	Electron transfer	Doxycycline	$[Doxycycline]_0$ = 10.0 mg L^{-1}, 300 W xenon lamp	Dissolved oxygen	•O_2^-	94.2% (1.0 h)	72.0%	[25]
BMO-3	Electron transfer	APAP	$[APAP]_0$ = 20.0 μmol L^{-1}, 300 W Xenon lamp, pH = 6.8	Dissolved oxygen	H_2O_2	96.0% (2.0 h)	61.0%	[27]
FT-200	Electron transfer	2,4-DCP	$[2,4\text{-}DCP]_0$ = 20.0 μmol L^{-1}, 300 W Xenon lamp, pH = 3.0	Dissolved oxygen	H_2O_2, •OH	100.0% (6.0 min)	91.5%	[28]
N-GQDs/ $Bi_2Fe_4O_9$	Electron transfer	BPA	$[BPA]_0$ = 20.0 mg L^{-1}, 300 W Xenon lamp, pH = 3.0	Dissolved oxygen	•OH	99.8% (90.0 min)	-	[29]
Sv-MoS_2/BN-5	Electron transfer	*E. coli*	$[E.\ coli]_0 = 6.0 \times 10^7$ CFU mL^{-1}, 300 W Xenon lamp, pH = 3.0	Dissolved oxygen	H_2O_2	100.0% (60.0 min)	-	[35]
CZS-5	Electron transfer	phenol	$[phenol]_0$ = 20.0 mg L^{-1}, 300 W Xenon lamp, pH = 7.0	O_2 aeration	H_2O_2	97.6% (180.0 min)	87.0%	[36]
Cv-PCNNS	Electron transfer	MTZ	$[MTZ]_0$ = 10.0 mmol L^{-1}, 300 W Xenon lamp, pH = 7.0	O_2 aeration	H_2O_2, •OH	90.7% (100.0 min)	62.0%	[47]
g-C_3N_4	Electron transfer	TC	$[TC]_0$ = 50.0 ppm, 300 W Xenon lamp, pH = 7.0	Dissolved oxygen	H_2O_2, •OH	90.0% (300 min)	-	[48]
FeOOH/UPCN	Electron transfer	OTC	$[OTC]_0$ = 20.0 mg L^{-1}, 300 W Xenon lamp, pH = 7.0	Dissolved oxygen	H_2O_2, •OH	86.2% (120.0 min)	48.6%	[49]

Note: "Dissolved oxygen" refers to the oxygen that comes from the dissolved oxygen in the aqueous solution without any aeration; "Air aeration" refers to the main source of oxygen in the system from the air; "O_2 aeration" signifies that the primary source of oxygen in the system is pure oxygen. Abbreviations: OV-BOC, BiOCl with oxygen vacancy; BWO, Bi_2WO_6; Nd-BiO_{2-x}, Nd doped BiO_{2-x}; BMO-3, iodine-doped Bi_2MoO_6; FT-200, Fe_2O_3 loaded TiO_2 nanoparticles; N-GQDs/$Bi_2Fe_4O_9$, nitrogen-doped graphene quantum dots/$Bi_2Fe_4O_9$; Sv-MoS_2/BN-5, sulfur vacancy-rich MoS_2/boron nitride; CZS-5, N-doped hollow carbon spheres/$Zn_2In_2S_5$; Cv-PCNNS, porous g-C_3N_4 nanosheets with carbon vacancies; g-C_3N_4, graphitic carbon nitride; FeOOH/UPCN, iron-based oxyhydroxides/ultrathin porous g-C_3N_4; RhB, rhodamine B; NaPCP, sodium pentachlorophenate; APAP, acetaminophen; 2,4-DCP, 2,4-dichlorophenol; BPA, bisphenol A; *E. coli*, *Escherichia coli*; MTZ, metronidazole; TC, tetracycline; OTC, oxytetracycline.

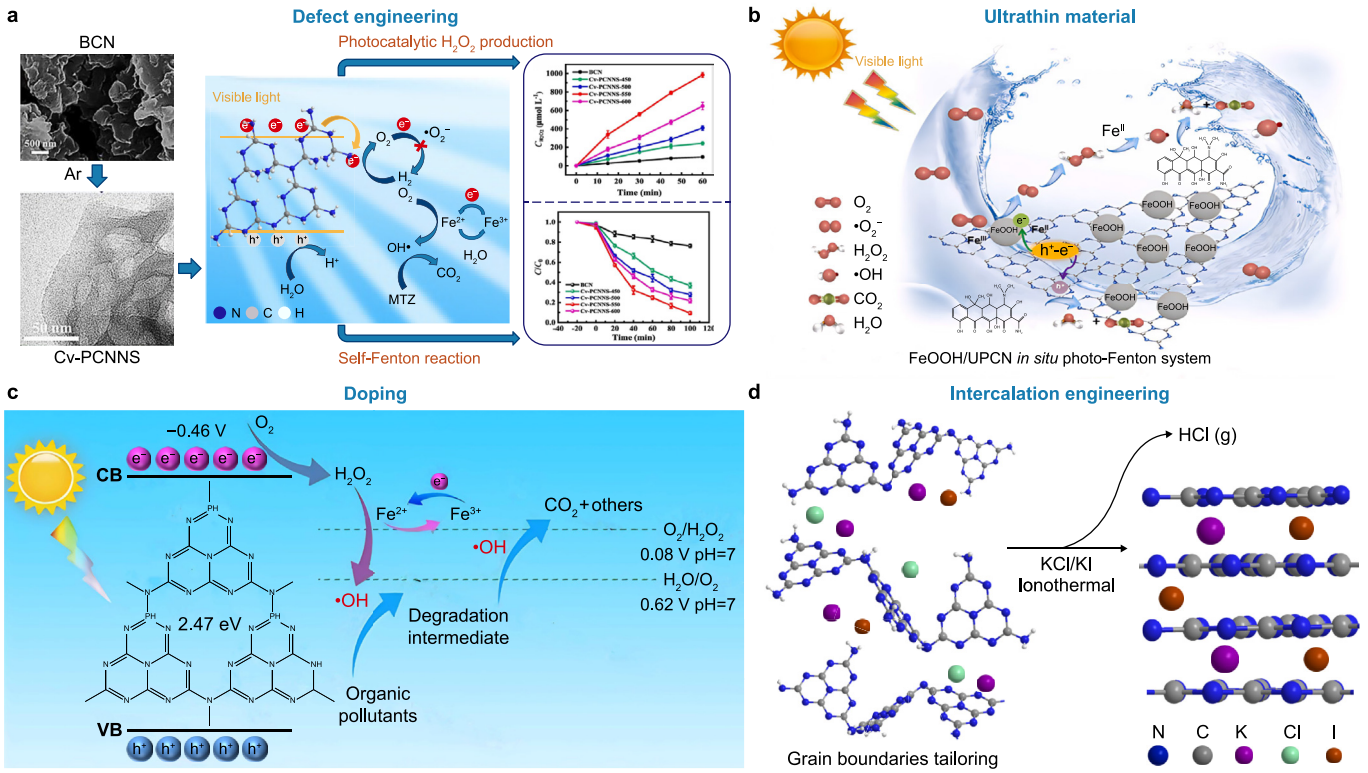

Fig. 1. **a**, Proposed mechanism for the photocatalysis-self-Fenton system based on carbon defective Cv-PCNNS-550. Reproduced with permission from Ref. [47]. Copyright 2023, Elsevier. **b**, The photo-Fenton degradation mechanism proposed in the FeOOH/UPCN composite system with ultrathin material. Reproduced with permission from Ref. [49]. Copyright 2022, Elsevier. **c**, Mechanism for the photocatalysis-self-Fenton system of P doped g-C_3N_4. Reproduced with permission from Ref. [50]. Copyright 2020, Elsevier. **d**, The ionothermal synthesis of K^+/I^- intercalated g-C_3N_4 (CN-KCl/KI). Reproduced with permission from Ref. [52]. Copyright 2023, NAS.

produced via the oxygen reduction. Inefficient carrier separation negatively affects O_2 activation, particularly during electron transfer processes. To address this issue, doping has emerged as an effective strategy for enhancing carrier separation and ensuring efficient O_2 activation. An oxygen-doped g-C_3N_4 (OCN) variant has been synthesized, resulting in a 3.5-fold increase in H_2O_2 production under monochromatic light compared to bulk g-C_3N_4 [51]. The improved carrier transfer efficiency in OCN facilitates the two-electron reduction of O_2 and consequently demonstrates superior degradation efficiencies for phenol and 2,4-DCP.

Intercalation engineering in carbon nitride significantly improves carrier separation and transfer, enhancing O_2 activation for H_2O_2 production. In a recent study, Liu et al. [52] modified g-C_3N_4 by the intercalation of potassium ions (K^+) and iodide ions (I^-) into its layered structure, resulting in the achievement of a H_2O_2 production rate of 13.1 mM g^{-1} h^{-1} and an apparent quantum yield of 23.6% at 400 nm for this ion-intercalated crystalline g-C_3N_4. This suggests that interstitial doping engineering can facilitate the creation of rapid charge diffusion channels and promote efficient two-electron oxygen reduction (Fig. 1d).

In summary, the photocatalytic activation of O_2 has been extensively investigated and applied in environmental purification. The protocol eliminates the need for additional oxidants during the process. Moreover, this procedure can generate various ROS, which are advantageous for the degrading and mineralizing organic pollutants. Photocatalytic reactions typically occur at room temperature, with simple operation and without requiring complex equipment or conditions. However, the efficiency of photocatalytic O_2 activation is limited by factors such as charge carrier recombination, low carrier migration rate, and insufficient activated O_2 adsorption sites. Although certain emerging catalysts can overcome these challenges, they often increase production costs. Additionally, prolonged usage leads to catalyst deactivation or breakdown, necessitating periodic replacement or regeneration, escalating costs and complicating operations. Current studies primarily employ artificial illumination for photocatalysis; however, this approach is energy-intensive. While the photocatalytic activation of O_2 to generate ROS holds promise for pollutant eradication, further investigation is needed to overcome existing obstacles and enhance its practicability and efficacy.

3. Chemical oxygen activation

The activation of O_2 through photochemistry requires strict conditions, including temperature, light radiation intensity, photoreactor design, and selection of photocatalytic materials [53,54]. These limitations may hinder the broader application of photocatalytic O_2 activation. Conversely, certain zero-valent metals (ZVMs), low-valent transition metals (LVTMs), and defect materials can activate O_2 without such demanding operating environments.

3.1. Zero valent metals

In recent years, the potential of ZVMs, such as Fe, Al, and Cu, to activate O_2 has gained increasing recognition due to their ability to generate various ROS for pollutant removal. Notably, zero-valent iron (ZVI, Fe^0) has garnered significant attention owing to its safety and widespread availability [55]. When introduced into a solution containing dissolved oxygen, Fe^0 undergoes a thermodynamically spontaneous corrosion reaction. This process involves electron transfer from Fe^0 to O_2, leading to the oxidation of Fe^0 into Fe^{2+}. Concurrently, O_2 is reduced to H_2O_2. In acidic or neutral

environments, Fe^{2+} further catalyzes H_2O_2 formation into •OH (equations (1) and (2)).

$$Fe^0 + O_2 + 2H^+ \rightarrow Fe^{2+} + H_2O_2 \quad (1)$$

$$Fe^{2+} + H_2O_2 \rightarrow Fe^{3+} + \bullet OH + OH^- \quad (2)$$

Numerous studies have established that ROS generated from the activation of O_2 by Fe^0 predominantly consists of H_2O_2, thus making this process analogous to a Fenton-like reaction. The Fe^0/O_2 system has been used for treating refined cottonseed oil (CTO) wastewater (Fig. 2a) [56]. Experimental findings have demonstrated the effective degradation of CTO in wastewater using the Fe^0/O_2 system with an observable enhancement in degradation efficiency due to increased oxygen concentration. To further enhance the degradation efficiency and prevent Fe^0 aggregation within this system, researchers have developed composite materials by combining Fe^0 with other substances. Carbon-coated nano ZVI (Fe@C), obtained by high-temperature calcination of complexes formed between Fe and organic compounds, exhibit small size, high content, and excellent dispersion properties, ensuring their heightened activity in Fenton-like reactions [57]. This catalyst activates O_2 to generate H_2O_2 and forms the Fe@C-H_2O_2 Fenton system, effectively degrading SMT. Yang et al. [58] encapsulated nano ZVI within a three-dimensional graphene network material (3D-GN@nZVI), successfully activating dissolved oxygen and facilitating sulfadiazine (SDZ) degradation. In addition, introducing foreign metals can accelerate the corrosion of Fe^0 and enhance the efficiency of O_2 activation [59].

Similar to ZVI, zero valence copper (ZVC, Cu^0) can also activate O_2, leading to the production of H_2O_2 and the formation of a Fenton-like system. Meanwhile, during the oxidation process, Cu^0 generates Cu^+ and Cu^{2+} ions, which subsequently react with *in situ* generated H_2O_2 to produce •OH and $\bullet O_2^-$ radicals (equations (3)–(5)).

$$2Cu^0 + O_2 + H_2O_2 \rightarrow 2Cu^+ + H_2O_2 + 2OH^- \quad (3)$$

$$Cu^+ + H_2O_2 \rightarrow 2Cu^{2+} + \bullet OH + 2OH^- \quad (4)$$

$$Cu^{2+} + O_2 + H_2O_2 \rightarrow Cu^+ + \bullet O_2^- + H^+ \quad (5)$$

The involvement of Cu^+ and Cu^{2+} ions adds complexity to the process of Cu^0 activating O_2. In an nZVC/air system, nZVC can activate O_2 to produce H_2O_2 while simultaneously releasing Cu^+ [60]. This activation further catalyzes the transformation of H_2O_2 into •OH and facilitates the destruction of -N=N- azo pollutants, forming carbon-centered radicals. Both radicals contribute to mineralizing low molecular weight organic acids under neutral conditions. Cu^0 exhibits significant potential for activating O_2 and removing organic pollutants. However, Cu^0 tends to aggregate and release a large amount of copper ions after use during its preparation process, leading to contamination in water environments and reducing its catalytic activity [61]. Additionally, factors such as dissolved oxygen concentration and mass transfer efficiency also influence the catalytic performance of Cu^0. To address these issues, Yang et al. [62] developed a novel mesoporous carbon-hybridized zero-valent copper (Cu^0/C) through the calcination of copper-based metal-organic frameworks ($Cu_3(BTC)_2$) in a tubular furnace (Fig. 2b). The carbon-based matrix not only adsorbs pollutants but also effectively inhibits the leaching of copper ions. Under neutral pH conditions, the Cu^0/C-air system achieved a high SMT mineralization rate (73.1%). Table 2 lists ZVMs/O_2 systems for the degradation of contaminants.

Additionally, zero-valent zinc (ZVZ, Zn^0) can facilitate the *in situ* generation of H_2O_2 through the activation of O_2. However, the concentration of H_2O_2 generated by the Zn^0/air system is relatively low, necessitating further modifications to enhance its *in situ* generation [63]. According to electrochemical corrosion theory, Zn^0 acts as an anode in a corrosion cell, releasing electrons that are transferred to the cathode. The received electrons on the cathode surface can react with O_2 to produce H_2O_2. Simultaneously, Zn^0 undergoes oxidation, leading to the formation of precipitates such as ZnO or $Zn(OH)_2$, as depicted by equations (6)–(10).

$$2Zn + 3O_2 + 4H^+ \rightarrow H_2O_2 + 2ZnO + Zn(OH)_2 \quad (6)$$

$$\text{Anode}: Zn + 2e^- \rightarrow Zn^{2+} \quad (7)$$

$$\text{Cathode}: O_2 + 2H^+ + 2e^- \rightarrow H_2O_2 \quad (8)$$

$$Zn + H_2O_2 \rightarrow ZnO + H_2O \quad (9)$$

$$Zn^{2+} + H_2O_2 + 2e^- \rightarrow Zn(OH)_2 \quad (10)$$

Therefore, selecting suitable cathode materials is crucial for improving the efficiency of O_2 activation and increasing H_2O_2 production. Among various materials, carbon nanotubes (CNTs) have emerged as a standout choice due to their cost-effectiveness, high conductivity, and stability, making them widely utilized in electrochemical oxidation and fuel cell applications for *in situ* H_2O_2 generation [64,65]. Gong et al. [66] developed the Zn-CNTs-O_2 system wherein Zn and CNTs form a corrosion cell that reduces O_2 to H_2O_2 on CNTs' surface (Fig. 2c). Simultaneously, dissolved Zn^{2+} precipitates as $Zn(OH)_2$ onto the CNTs. The formation of this corrosion cell is primarily responsible for increasing the yield of H_2O_2. To further enhance the operational efficiency of the Zn/CNTs corrosion battery, some researchers have incorporated iron oxide and iron ions into Zn-CNTs. Liu et al. [67] synthesized a catalyst named Zn^0-CNTs-Fe_3O_4, which achieved a degradation rate of 98.6% toward OTC. Furthermore, combining zinc with iron yields superior outcomes; a Zn-Fe-CNTs catalyst based on Zn^0-CNTs and Fe^0 eliminated sulfamethoxazole (SMX) within just 10.0 min [68].

3.2. Low valence transition metals

In contrast to ZVMs, certain LVTMs also function as electron donors for the activation of O_2, resulting in the generation of ROS. Among these LVTMs, extensive research has been conducted on the activation of O_2 by Fe^{2+}. Fe^{2+} can activate dissolved oxygen under aerobic conditions, leading to the formation of $\bullet O_2^-$, which subsequently accepts electrons and ultimately leads to the generation of H_2O_2. Moreover, Fe^{2+} plays a crucial role in the Fenton reaction with H_2O_2, facilitating the production of •OH [70]. This mechanism exhibits high efficacy in degrading organic pollutants, according to equations (11)–(13).

$$Fe^{2+} + O_2 \rightarrow Fe^{2+} + \bullet O_2^- \quad (11)$$

$$Fe^{2+} + \bullet O_2^- + 2H^+ \rightarrow Fe^{3+} + H_2O_2 \quad (12)$$

$$Fe^{2+} + H_2O_2 + H^+ \rightarrow Fe^{3+} + \bullet OH + H_2O \quad (13)$$

In a neutral environment, forming irreversible precipitates by Fe^{3+} impedes the activation of O_2 and the generation of ROS. Additionally, reducing Fe^{3+} to Fe^{2+} is a slow process mediated by $\bullet O_2^-$, resulting in low efficiency and limiting the removal of pollutants. Researchers have explored incorporating ligands into O_2 activation

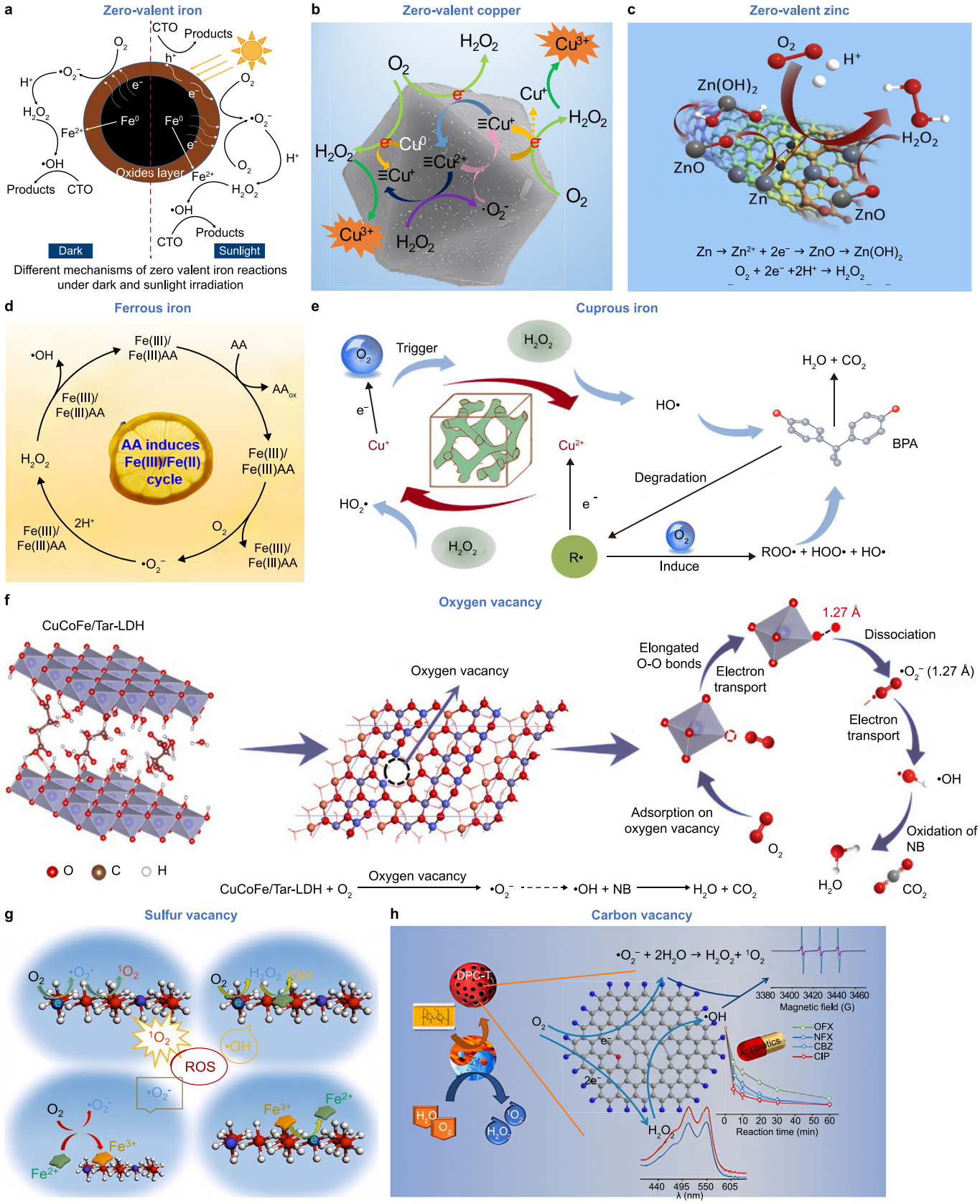

Fig. 2. **a**, The degradation mechanisms of CTO by ZVI system. Reproduced with permission from Ref. [56]. Copyright 2022, Elsevier. **b**, The degradation mechanism of SMT in the Cu^0/C-air system. Reproduced with permission from Ref. [62]. Copyright 2021, Elsevier. **c**, Mechanism for active species generation in the Zn^0-CNTs-O_2 system. Reproduced with permission from Ref. [66]. Copyright 2017, Elsevier. **d**, Ascorbic acid enhances the activation of oxygen by the Fe^{2+}/air process. Reproduced with permission from Ref. [71]. Copyright 2016, Elsevier. **e**, Mechanisms of activating O_2 by Cu(I) on Cu-Al/KIT-6. Reproduced with permission from Ref. [73]. Copyright 2020, Elsevier. **f**, Degradation mechanism of

systems to enhance pollutant removal efficiency to facilitate ROS production. Hou et al. [71] established an AA/Fe(II)/air system. They discovered that ascorbic acid (AA) enhances the activation process of O_2 by Fe^{2+}, unveiling an accelerated production rate of ROS through its pivotal role in promoting the Fe^{2+}/Fe^{3+} cycle (Fig. 2d). Furthermore, Zong et al. [72] constructed a Fe(II)-tetrapolyphosphate (TPP)/air system, which demonstrated that TPP significantly enhances the activation of O_2 by Fe^{2+} and accelerates the reduction of Fe^{3+}.

In recent studies, the activation of O_2 by Cu^{+} has garnered significant attention. Wang et al. [73] synthesized Cu-Al/KIT-6 and utilized it for the activation of O_2 (Fig. 2e). The experimental findings demonstrated that Cu^{+} effectively activated O_2 and generated ROS, thereby facilitating BPA removal, revealing its potential as an O_2 activator. However, the environmental instability of Cu^{+} poses a challenge to activating O_2. Zheng et al. [74] synthesized a hydrothermal carbonaceous carbon material containing stable CuCl (CuCl-HTCC) to address this limitation. Their study revealed that CuCl-HTCC contained a substantial amount of stable Cu^{+}, which exhibited significantly higher efficiency in activating O_2 than unstable homogeneous reactions involving only Cu^{+}. Table 3 provides examples showcasing pollutant degradation by LVTMs through the activation of O_2.

3.3. Defect engineering

Defect engineering has become a prominent research focus due to its ability to directly activate O_2, making it an attractive area for investigation in water treatment applications. Defect engineering involves deliberately manipulating a catalyst's performance by introducing, regulating, and repairing internal defects such as lattice, vacancies, and surface flaws. This approach does not rely on external energy or sacrificial reagents [78].

The presence of OVs plays a crucial role in the activation of O_2, making them recognized for their exceptional capability and potential to revolutionize this field. Wu et al. [79] discovered that OVs are crucial in generating ROS by capturing electrons and forming $\bullet O_2^-$. Additionally, OVs without electrons can extract electrons from organic pollutants, degrading them and maintaining electrostatic equilibrium, resulting in a 32.0% degradation rate of BPA without requiring an additional oxidant PMS.

However, the rapid reversion of $\bullet O_2^-$ back to O_2 may explain the decreased degradation rates of pollutants. Addressing this phenomenon, Wang et al. [80] synthesized CuCoFe/Tar-LDH with OVs and provided an explanation for the process (Fig. 2f). They proposed that the process began with the adsorption of O_2 onto the OVs in CuCoFe/Tar-LDH, which is then converted into $\bullet O_2^-$ and subsequently transformed into $\bullet OH$. The study by Wang et al. underscores the effectiveness of oxygen vacancy-mediated catalysts in directly activating O_2 to generate highly reactive oxidizing species. Based on these findings, it can be inferred that ROS production during the activation of O_2 through OVs is directly influenced by the dissolved oxygen concentration. Research conducted by Wang et al. [81] investigated the regulatory mechanism and transformation pathway of ROS during the process of O_2 activation. Their findings revealed that under low dissolved oxygen concentration conditions, O_2 predominantly leads to forming $^1O_2$ and $\bullet O_2^-$. Conversely, as the concentration of dissolved oxygen increases, there is a more prominent conversion from O_2 to $\bullet OH$. This study demonstrates that the potential for selective ROS production can be controlled by adjusting dissolved oxygen levels. Their research holds significant value in advancing wastewater treatment.

Moreover, this process also exhibits significant antimicrobial properties. For instance, a form of magnesium oxide with surface OVs can directly generate $^1O_2$ and $\bullet O_2^-$ through the reaction between OVs and O_2, even in the absence of light. This catalyst has demonstrated outstanding antibacterial performance by effectively eliminating *E. coli* within 2 h [82]. Additionally, Prasanna et al. [83] found that zinc oxide enriched with OVs exhibited significant antibacterial properties due to the generation of ROS through the activation of surface OVs.

However, research on the activation of O_2 by sulfur vacancies is less prevalent than that on OVs. Ultrasonic treatment of CoS_{2-x} material led to numerous sulfur vacancies on its surface, which can reduce dissolved oxygen to $\bullet O_2^-$ (Fig. 2g) [85]. Consequently, continuous generation of $^1O_2$ occurs, effectively degrading organic pollutants. OVs and sulfur vacancies are specific forms of anionic vacancies that arise due to the absence of oxygen or sulfur lattice sites in metal oxides and metal sulfides. These vacancies possess the ability to effectively promote O_2 activation. However, they are prone to instability and metal leaching, limiting their practical applicability. Therefore, non-metal carbon materials featuring carbon vacancies have attracted considerable interest. Liu et al. [86] conducted a study wherein they synthesized a type of defective porous carbon (DPC) capable of adsorbing dissolved oxygen and activating it into $\bullet O_2^-$ and $^1O_2$ (Fig. 2h). The experimental findings suggest that the primary active center for chemisorption and direct conversion of dissolved oxygen into $\bullet O_2^-$ may be the non-diagonal cyclic structure of carbon vacancies. The activation of O_2 by defect engineering for degradation of organic contaminants is systematically summarized in Table 4.

Compared to the photocatalytic activation of O_2, the chemical oxygen activation modality offers operational simplicity, reduced material preparation expenditures, and superior O_2 activation effects, resulting in effective pollutant removal. However, ZVMs and LVTMs are fundamentally expendable materials characterized by single-use functionality and minimal reusability. Moreover, the instability of these materials may lead to the liberation of metal ions, posing a risk of secondary contamination. Additionally, in alkaline environments, the catalytic activity of ZVMs and LVTMs may be curtailed, impacting the efficiency of ROS production. In contrast to ZVMs and LVTMs, defect structures can reduce reaction barriers, promote O_2 activation, and enhance pollutant degradation efficiency. The utilization of defect engineering for O_2 activation represents an emerging and cutting-edge technological approach. Nonetheless, a lack of dedicated research reports is currently elucidating the process and mechanism underlying O_2 activation via defect engineering. While defect engineering is indispensable for O_2 activation, the accumulation of reaction intermediates, water, and other catalysts on the molecular surface may fill up defects, diminishing adsorption capacity toward O_2 while hindering electron transfer. The design and synthesis of defect materials with proficient activation properties pose a significant challenge, requiring careful consideration of catalyst architecture, composition, and synthesis techniques, potentially extending the trajectory of research and development.

4. Electrochemical oxygen activation

The electrochemical activation of O_2 is a pivotal pathway for the

nitrobenzene (NB) in air/CuCoFe/Tar-LDH reaction systems. Reproduced with permission from Ref. [80]. Copyright 2022, ACS. **g**, The mechanism of ROS generation in the $CoS_{2-1.5\ h}$ system. Reproduced with permission from Ref. [85]. Copyright 2021, Wiley. **h**, The oxygen molecule activation by carbon defects. Reproduced with permission from Ref. [86]. Copyright 2023, Elsevier.

Table 2
The removal of pollutants based on ZVMs/O_2 systems.

ZVMs	Contaminants	Reaction conditions	O_2 supply	ROS	Removal efficiency	TOC removal	Reference
ZVI	CTO	pH = 2.5–3.1	O_2 aeration	H_2O_2, •OH	93.5% (3.0 h)	-	[56]
Fe@C	SMT	$[SMT]_0$ = 20.0 mg L^{-1}, pH = 4.0	Dissolved oxygen	H_2O_2, •OH	97.6% (300.0 min)	93.8%	[57]
3D-GN@nZVI	SDZ	$[SDZ]_0$ = 10.0 mg L^{-1}, pH = 3.0	Dissolved oxygen	H_2O_2, •OH	81.0% (120.0 min)	-	[58]
BM Fe/Cu	4-CP	$[4\text{-}CP]_0$ = 20.0 mg L^{-1}, pH = 3.0	Air aeration	$•O_2^-$, •OH	100.0% (120.0 min)	66.4%	[59]
nZVC	MO	$[MO]_0$ = 20.0 mg L^{-1}, pH = 6.6	Air aeration	H_2O_2, •OH	100.0% (4.0 h)	56.1%	[60]
ZVCMMT	ATZ	$[ATZ]_0$ = 15.0 μM, pH = 3.0	Air aeration	•OH	90.0% (180.0 min)	-	[61]
Cu^0/C	SMT	$[SMT]_0$ = 20.0 m L^{-1}, pH = 4.0	Air aeration	H_2O_2, •OH	96.7% (90.0 min)	68.8%	[62]
Zn^0-CNTs-Fe_3O_4	OTC	$[OTC]_0$ = 100.0 mg L^{-1}, pH = 3.0	O_2 aeration	H_2O_2, •OH	98.6% (60.0 min)	-	[67]
Zn-Fe-CNTs	SMX	$[SMX]_0$ = 20.0 mg L^{-1}, pH = 1.50	O_2 aeration	H_2O_2, •OH	100.0% (120.0 min)	51.3%	[68]
ZVZ/Cu(II) system	MTZ	$[MTZ]_0$ = 10.0 mg L^{-1}, pH = 5.0	Dissolved oxygen	H_2O_2, •OH, $•O_2^-$	90.0% (10.0 min)	-	[69]

Abbreviations: ZVI, zero-valent iron; Fe@C, carbon-coated nanoscale zero-valent iron; 3D-GN@nZVI, nanoscale zero-valent iron encapsulated in three-dimensional graphene network; BM Fe/Cu, ball milling Fe/Cu; nZVC, nanoscale zero-valent copper; ZVCMMT, montmorillonite templated zero-valent copper; Cu^0/C, mesoporous carbon hybrid loaded zero-valent copper; Zn^0-CNTs-Fe_3O_4, Zn^0-carbon nanotubes-Fe_3O_4; Zn-Fe-CNTs, Zn-Fe-carbon nanotubes; ZVZ/Cu(II) system, zero-valent zinc/Cu(II) system; CTO, cottonseed oil; SMT, sulfamethazine; SDZ, sulfadiazine; 4-CP, 4-chlorophenol; MO, methyl orange; ATZ, atrazine; OTC, oxytetracycline; SMX, sulfamethoxazole; MTZ, metronidazole.

Table 3
The degradation of pollutants by LVTMs/O_2 systems.

LVTMs	Contaminants	Reaction conditions	O_2 supply	ROS	Removal efficiency	TOC removal	Reference
AA/Fe(II)	RhB	$[RhB]_0$ = 0.01 mmol L^{-1}, pH = 6.0	Air aeration	H_2O_2, •OH	47.0% (6.0 h)	16.0%	[71]
Fe(II)-TPP complex	SMX	$[SMX]_0$ = 1.3 mg L^{-1}, pH = 8.0	Air aeration	H_2O_2, •OH, $•O_2^-$	75.7% (20.0 min)	-	[72]
Cu-Al/KIT-6	BPA	$[BPA]_0$ = 25.0 mg L^{-1}, pH = 5.0	O_2 aeration	H_2O_2, •OH	99.0% (120.0 min)	46.0%	[73]
CuCl-HTCC	IBU	$[IBU]_0$ = 10.0 mg L^{-1}, pH = 4.6	Magnetic stirring	$•O_2^-$, •OH	Almost 100.0% (120.0 min)	-	[74]
P-Cu	IBU	$[IBU]_0$ = 10.0 mg L^{-1}, pH = 6.0	Air aeration	•OH	100.0% (120.0 min)	52.6%	[75]
Mo/Cu^{2+} system	IBU	$[IBU]_0$ = 5.0 ppm, pH = 3.0	Air aeration	$^1O_2$, $•O_2^-$	67.2%	-	[76]
Fe_3O_4/O_2/TPP system	PNP	$[PNP]_0$ = 10.0 mg L^{-1}, pH = 3.0	Dissolved oxygen	•OH	80.0% (480.0 min)	-	[77]

Abbreviations: AA/Fe(II), ascorbic acid/Fe(II); Fe(II)-TPP complex, Fe(II)-tetrapolyphosphate complex; Cu-Al/KIT-6, framework Cu doped Al_2O_3 dispersed on KIT-6; CuCl-HTCC, copper chloride loaded hydrothermal carbonaceous carbon; P-Cu, low valence copper on red P; Fe_3O_4/O_2/TPP system, Fe_3O_4/O_2/tripolyphosphate system; RhB, rhodamine B; SMX, sulfamethoxazole; BPA, bisphenol A; IBU, ibuprofen; PNP, *p*-nitrophenol.

Table 4
The activation of O_2 by defect engineering for degradation of organic contaminants.

Catalyst	Defect engineering	Contaminants	Reaction conditions	O_2 supply	ROS	Removal efficiency	TOC removal	Reference
Fe-Co LDH	Oxygen Vacancy	BPA	$[BPA]_0$ = 2.0 mg L^{-1}, pH = 7.0	Dissolved oxygen	$^1O_2$, $•O_2^-$	32.0% (60.0 min)	49.0%	[79]
CuCoFe/Tar-LDH	Oxygen Vacancy	NB	$[NB]_0$ = 150.0 mg L^{-1}, pH = 7.2	Air aeration	•OH, $•O_2^-$	78.3% (240.0 min)	45.5%	[80]
CuCoFe-300	Oxygen Vacancy	CIP	$[CIP]_0$ = 15.0 mg L^{-1}, pH = 4.0	O_2 aeration	•OH, $•O_2^-$	75.0% (240.0 min)	54.1%	[81]
MgO	Oxygen Vacancy	*E. coli*	$[E.\ coli]_0$ = 0.05 mol L^{-1}, pH = 8.0	O_2 aeration	$•O_2^-$, $^1O_2$	100.0% (2.0 h)	-	[82]
ZnO	Oxygen Vacancy	*S. aureus*	$[S.\ aureus]_0$ = 3.0 × 10^{12} CFU mL^{-1}, pH = 8.5	Dissolved oxygen	•OH, $•O_2^-$, H_2O_2	17.0% (120.0 min)	-	[83]
DR-MoS_2	Sulfur vacancy	Black T	$[Black\ T]_0$ = 10.0 mg L^{-1}, pH = 3.0	Dissolved oxygen	•OH, H_2O_2	99.8% (25.0 min)	-	[84]
CoS_{2-x}	Sulfur vacancy	RhB	$[RhB]_0$ = 20.0 mg L^{-1}, pH = 4.5	Dissolved oxygen	$^1O_2$	91.9% (120.0 min)	70.7%	[85]
DPC-800	Carbon vacancy	CIP	$[CIP]_0$ = 20.0 mg L^{-1}, pH = 6.6	Dissolved oxygen	$^1O_2$, $•O_2^-$	98.0% (60.0 min)	-	[86]

Abbreviations: Fe-Co LDH, Fe-Co layered double hydroxide; CuCoFe/Tar-LDH, tartrate-modified CuCoFe-layered double hydroxide; CuCoFe-300, calcined CuCoFe-layered double hydroxide with 300 °C; DR-MoS_2, defect-rich MoS_2; DPC-800, calcined defected porous carbon with 800 °C; BPA, bisphenol A; NB, nitrobenzene; CIP, ciprofloxacin; *E. coli*, *Escherichia coli*; *S. aureus*, *Staphylococcus aureus*; Black T, Eriochrome Black T; RhB, rhodamine B.

in situ synthesis of H_2O_2, playing a significant role in various processes. At the cathode, O_2 undergoes a two-electron reduction reaction to produce H_2O_2. The presence of catalysts or electrons influences the catalytic decomposition of H_2O_2 into various ROS. Based on the mode of ROS formation, the electrochemical activation of oxygen can be further categorized into four processes: the electro-Fenton (EF) process, the photoelectro-Fenton (PEF) process, the photoelectrocatalytic (PEC) process, and the microbial fuel cell (MFC) process.

4.1. Electro-Fenton process

The EF process involves the introduction of O_2 or air at the cathode, facilitating the continuous *in situ* generation of H_2O_2 through $2e^-$ oxygen reduction reaction (ORR) (Fig. 3a). The incorporation of the Fe^{2+} catalyst within the Fenton reaction leads to the generation of •OH (equations (14) and (15)). •OH indiscriminately degrades organic pollutants into smaller organic molecules, salts, and carbon dioxide via addition, substitution, and bond cleavage.

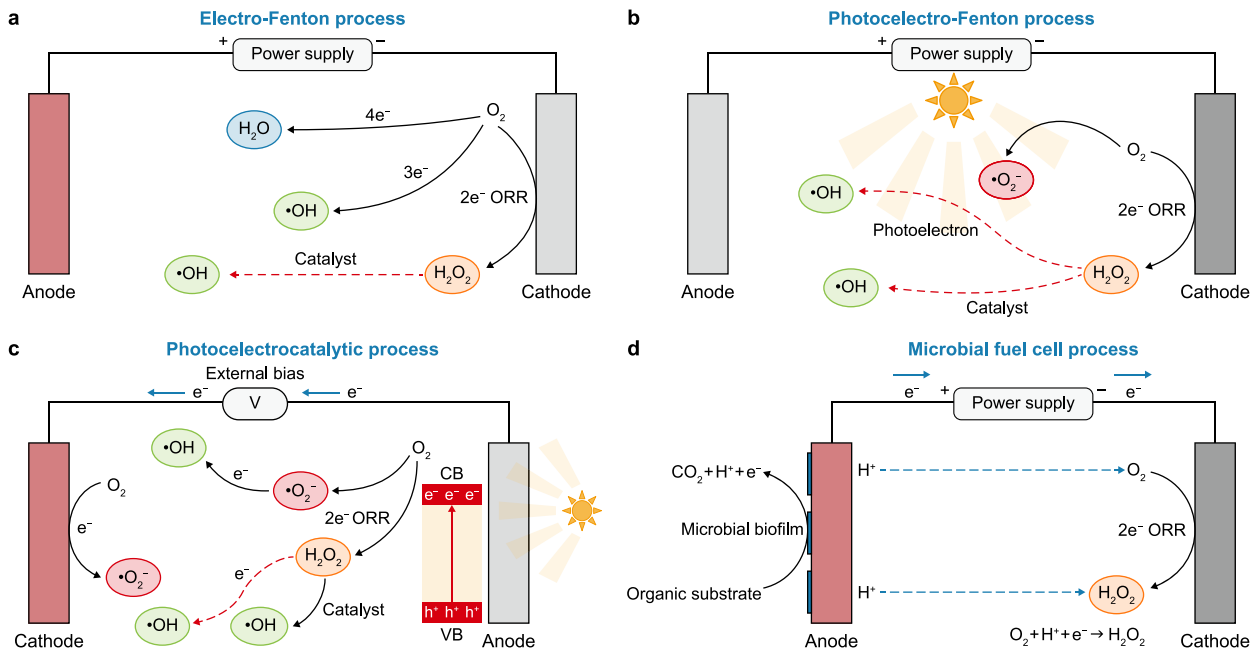

Fig. 3. The ROS generation pathway based on the activation of O_2 by electro-Fenton process (**a**), photoelectro-Fenton process (**b**), photoelectrocatalytic process (**c**), mcrobial fuel cell process (**d**).

Variations in reaction conditions, including pH, cathode material, and anode catalyst, can result in distinct mechanisms and efficiencies in the EF reaction.

$$O_2 + 2H^+ + 2e^- \rightarrow H_2O_2 \quad (14)$$

$$O_2 + 3H^+ + 3e^- \rightarrow \bullet OH + H_2O \quad (15)$$

$$O_2 + 4H^+ + 4e^- \rightarrow 2H_2O \quad (16)$$

Zhao et al. [87] documented a FeCuC-embedded carbon aerogel with ORR activity, demonstrating high efficiency in removing organic pollutants through the EF reaction. By rapidly oxidizing surface Fe^0 to Fe^{2+}, this material facilitated the generation of •OH from H_2O_2, resulting in a significant removal rate of TOC for various organic pollutants (88–99%). Moreover, other metals, such as Co^{2+} and Fe^{2+}, were found to catalyze H_2O_2 effectively in an R-FPE system used for degrading 2,4-DCP [88]. The synergistic effect between Co^{2+} and Fe^{2+} led to the abundant production of •OH by transforming electrochemically generated H_2O_2. However, several challenges currently hinder the EF process, including the limited availability of selective and active catalysts, suboptimal H_2O_2 synthesis via the two-electron ORR pathway, the reduced efficacy of H_2O_2 decomposition through the Haber–Weiss cycle, and sluggish activation of catalytic metal sites [89]. Fortuitously, the emergence of single-atom catalyst (SAC) membranes has been shown to augment two-electron ORR, thereby facilitating the conversion of H_2O_2 into •OH via one-electron ORR. This advancement improves degradation efficiency and the system's stability [90]. Jin et al. [91] successfully developed a p-block BiN_3/MXene electrocatalytic membrane that proficiently executes a three-electron ORR to generate •OH from O_2. Without additional chemical reagents, this novel approach achieves a maximum production rate of 26.7 μmol L^{-1} h^{-1} cm^{-2} for •OH and an observed rate constant (K_{obs}) for SMX degradation reaching 1.03 min^{-1}.

The cathodic surface can generate H_2O_2 through a two-electron reduction pathway or water via a direct four-electron pathway (equation (16)), depending on the type and intrinsic properties of the cathode material and other operating conditions. The selectivity of the cathode material for the ORR is crucial in achieving the *in situ* generation of H_2O_2 at the cathodic interface, particularly when compared to metallic substrates. Carbon-based materials are considered more suitable for the *in situ* synthesis of H_2O_2 due to their distinct features, including enhanced stability, minimal toxicity, affordability, corrosion resistance, and pronounced selectivity for the two-electron pathway in O_2 reduction. To activate O_2 efficiently, a large-pore graphene aerogel (GA) cathode with a substantial surface area has been utilized [92]. Abundant large pores served as reactive sites facilitating the efficient generation of •OH through the electrochemical decomposition of Fe^{2+}, producing H_2O_2 (107.6 mg L^{-1}), resulting in a ciprofloxacin (CIP) TOC removal rate of 91.0%. Gu et al. [93] employed oxygen-doped CNTs (OCNT) as cathodes to catalyze O_2 activation for the degradation of organic pollutants.

Within O_2-activated EF systems, H_2O_2 and •OH are the primary ROS. However, •OH has a short lifespan and limited selectivity. In contrast, metastable $^1O_2$, which possesses unoccupied π* orbitals, can selectively target electron-rich micropollutants through electrophilic addition. Therefore, investigating EF systems for generating $^1O_2$ is of particular significance. Jin et al. [94] developed a fluidic single-atom electrode specifically designed for the selective electrocatalysis of O_2 into $^1O_2$. This system achieved an impressive selectivity of over 98.0% for $^1O_2$ production and a removal rate of SMX of 91.9%. Yang et al. [95] engineered a conductive electrocatalytic membrane with Fe(II)-modulated FeCo-layered double hydroxide nanosheets (Fe(II)-FeCo LDHs). These nanosheets effectively catalyzed H_2O_2 into $^1O_2$, exhibiting high kinetic activity with a rate constant of 0.04 min^{-1} and achieving a degradation efficiency of 93.2% for atrazine (ATZ). The selective production of $^1O_2$ is crucial in precise chemical site targeting. Feng et al. [96] proposed a novel strategy to construct an oxidation–reduction interface on the electrode surface. They discovered that this strategy predominantly generated $^1O_2$, effectively circumventing the competitive formation of other ROS. By leveraging a cutting-edge carbon-based

electrocatalytic bilayer system, which takes advantage of the synergistic effect of dual active electrochemical membrane electrodes, they enhanced the production $^1O_2$ [97]. The optimized production of $^1O_2$ achieved a concentration of 2583.0 μmol L^{-1} without additional chemical reagents. This system accomplished a propranolol (PRO) removal efficiency of 97.5%. Table 5 lists the recent studies on the degradation of contaminants in water or wastewater by the EF process.

4.2. Photoelectro-Fenton process and photoelectrocatalytic process

The PEF process is an advanced oxidation method combining photocatalytic and electrochemical reactions. By integrating the properties of photocatalysis with electrochemical oxidation, the dual-functional PEF catalysts synergistically exploit photoelectric properties, effectively accelerating the recycling of Fe^{2+}/Fe^{3+} in traditional electrochemical reactions, expanding the operational pH range, and simultaneously maintaining elevated degradation efficiencies (Fig. 3b). Bai et al. [98] developed a novel PEF-like system utilizing a bifunctional Z-scheme $WO_3/g\text{-}C_3N_4$ catalyst, which significantly accelerated the degradation of CIP. The PEF system exhibited superior efficacy in removing CIP compared to singular photocatalytic and EF systems, achieving complete elimination within just 2 h under visible light irradiation.

In the PEF process, various ROS can be generated through light and electric reactions. Wang et al. [99] developed an integrated system based on zinc-air batteries that incorporate polyterthiophene (pTTh) as a photo-enhanced electrocatalyst, achieving a high H_2O_2 production rate (34.8 mg L^{-1} h^{-1}) and effectively degrading co-generated pollutants through efficient catalysis of the $2e^-$ ORR. Compared to the EF process, PEF generates •OH and H_2O_2 and produces active substances such as e^-, h^+, and $\bullet O_2^-$, resulting in a broader spectrum of ROS that facilitates the effective breakdown of stubborn organic pollutants. Du et al. [100] synergized UV irradiation and heterogeneous electro-Fenton (Hetero-EF) treatment by employing FeCu@PC porous carbon, adeptly reducing O_2 in the Hetero-PEF process with a TOC removal rate of 73.3% for SMT, which is 2.2 times higher than that achieved by the Hetero-EF process. Sunlight is the most cost-effective illumination compared to costly artificial light sources in PEF. Therefore, solar-powered PEF (SPEF) is a more viable alternative to conventional PEF. Ye et al. [101] discovered that SPEF outperformed electrooxidation (EO), EF, and UVA (ultraviolet with wavelength 320–400 nm) -assisted PEF in efficiently degrading bronopol under a consistent current density. After 360 min of operation, SPEF realized a mineralization rate of 94.0%. Pinheiro et al. [102] utilized Fe_3O_4 nanoparticles as heterogeneous catalysts to initiate SPEF, which exhibited a catalytic removal efficiency of 98.7% for fuel within just 90.0 min. Salmerón et al. [103] conducted an inaugural pilot-scale experiment of SPEF, meticulously engineering the experimental apparatus to optimize the electrocatalytic synthesis of H_2O_2. By fine-tuning the conditions, they achieved an H_2O_2 production rate of 64.9 mg min^{-1} with a current efficiency of 89.3%. The SPEF process facilitated rapid degradation of over 50.0% of pesticide residues within a mere 5.0 min.

The PEC process combines the principles of photocatalysis and electrochemical oxidation, synergistically enhancing charge carrier segregation and reducing recombination events upon illumination (Fig. 3c). In contrast to the PEF paradigm, an electrical bias is strategically applied in the PEC system to mobilize photoelectrons for oxygen reduction at the cathode [104]. Simultaneously, photogenerated holes migrate to the anode's surface, generating highly oxidative and indiscriminate •OH, while electrons catalyze additional oxidants. Apart from •OH and hole, other oxidizing entities such as $\bullet O_2^-$ and perhydroxyl radicals are also present in the PEC system, as described by equations (17)–(21) [105,106].

$$hv + \text{semiconductor} \rightarrow h^+ + e^- \tag{17}$$

$$h^+ + H_2O \rightarrow \bullet OH + H^+ \tag{18}$$

$$e^- + O_2 \rightarrow \bullet O_2^- \tag{19}$$

$$\bullet O_2^- + H^+ \rightarrow \bullet HO_2 \tag{20}$$

$$2 \bullet HO_2 \rightarrow H_2O_2 + O_2 \tag{21}$$

In the PEC-based WO_3/FPC system, an anodic potential was applied to the WO_3 photoanode, facilitating the segregation of photogenerated charges. Meanwhile, the F-doped porous carbon served as the cathode and was selectively designed to catalyze the reduction of O_2 to H_2O_2 [107]. This system measured an H_2O_2 generation rate of 0.87 mmol L^{-1} h^{-1} with a Faradaic efficiency (FE) of 75.0%. The degradation rates of phenol, BPA, and ATZ exceeded

Table 5
The pollutants degradation based on the activation of O_2 by electro-Fenton process.

Cathodes	Anodes	Contaminants	Reaction conditions	O_2 supply	ROS	Removal efficiency	TOC removal	Reference
FeCuC	BDD	BPA	$[BPA]_0$ = 2.0 mg L^{-1}, Na_2SO_4 = 50.0 μM, I = 30.0 mA, pH = 3.0	O_2 aeration	H_2O_2, •OH	-	97.0%	[87]
GF-C	Pt	RhB	$[RhB]_0$ = 60.0 mg L^{-1}, Na_2SO_4 = 50.0 μM, j = 6.0 mA cm^{-2}, pH = 3.0	O_2 aeration	H_2O_2, •OH	99.0%	80.0%	[88]
Ti sheet	BiN_3/MXene membrane	SMX	$[SMX]_0$ = 10.0 mg L^{-1}, Na_2SO_4 = 20.0 mmol L^{-1}, I = 10.0 mA, pH = 3.0–9.5	O_2 aeration	H_2O_2, •OH	>95.0%	60.0%	[91]
GA	Pt sheet	CIP	$[CIP]_0$ = 50.0 mg L^{-1}, Na_2SO_4 = 50.0 μM, j = 30.0 mA cm^{-2}, pH = 3.0,	O_2 aeration	H_2O_2, •OH	Almost 100.0%	91.0%	[92]
CrN4/ MXene	Ti sheet	SMX	$[SMX]_0$ = 10.0 mg L^{-1}, pH = 6.8	O_2 aeration	$^1O_2$	95.0%	61.2%	[94]
FE-ECM	Titanium plate	ATZ	$[ATZ]_0$ = 20.0 μM, Na_2SO_4 = 100.0 mM, j = 2.0 mA cm^{-2}, pH = 7.0	O_2 aeration	H_2O_2, •OH, $^1O_2$	93.1%	73.04%	[95]
Carbon aerogels	Pt foil	BPA	$[BPA]_0$ = 10.0 mg L^{-1}, Na_2SO_4 = 50.0 μM, pH = 3.0 and 9.0	O_2 aeration	H_2O_2, $^1O_2$, $\bullet O_2^-$, •OH	98.0%	72.3%	[96]
MOF-SnO_2@CF	Fe@CF membranes	PRO	$[PRO]_0$ = 5.0 mg L^{-1}, Na_2SO_4 = 10.0 μM, pH = 3.0	O_2 aeration	H_2O_2, $^1O_2$, $\bullet O_2^-$, •OH	97.5%	83.0%	[97]

Abbreviations: FeCuC, iron-copper-embedded carbon aerogel; BDD, boron-doped diamond; GF-C, graphite felt-C; GA, graphene aerogel; FE-ECM, Fe(II)-modulated FeCo LDHs on a conductive OCNT-precoated membrane; MOF-SnO_2@CF, metal organic frameworks-SnO_2@ carbon fibers; Fe@CF, Fe@carbon fibers; BPA, bisphenol A; RhB, rhodamine B; SMX, sulfamethoxazole; CIP, ciprofloxacin; ATZ, atrazine; PRO, propranolol.

90.0% within 60.0 min, achieving a mineralization rate of 40.0%. Kaushik et al. [108] pioneered the development of a Fe_3O_4@Ni-CO_2O_4 (FNCO) photoanode, which was subsequently integrated into a PEC system. The designed PEC water treatment system achieved nearly 60.0% TOC removal efficiency. Furthermore, compared with electrochemical oxidation processes that require higher cell potentials for organic compound mineralization [109,110], one notable advantage of PEC systems is their lower bias potential requirement. Liang et al. [111] proposed a novel separated PEC system utilizing black TiO_2 nanospheres (b-TiO_{2-x}) as the photoanode. This innovative system demonstrated exceptional water purification efficacy (98.3%) and H_2O_2 synthesis (6.8 μmol h^{-1} cm^{-2}), operating at an impressively low voltage of 0.5 V while maintaining minimal energy expenditure for wastewater treatment at only 0.03 kWh m^{-3}. Zhang et al. [112] employed a magnetic Fe_3O_4@SiO_2@mesoporous TiO_2 (FST) photocatalyst-imbued electrode to implement a synergistic PEC/H_2O_2 process for the degradation of organic contaminants. In this FST PEC/H_2O_2 system, the removal rates of TOC within 8 min were found to be 77.9% (RhB), 80.2% (MO), and 65.5% (AMX). However, recent advancements in PEC technology have led to the development of a bias-free system capable of simultaneously synthesizing H_2O_2 and harvesting electrical energy [113]. Chen et al. [114] revealed that, upon visible light exposure, the WO_3/W photoanode induced a negative bias on the Pt/PVC photoelectrode while concurrently bestowing a positive bias upon the WO_3/W photoanode. The collaborative separation of hole-electron pairs across these dual photoelectrodes created an inherent bias. Jeon et al. [115] successfully synthesized pristine H_2O_2 solution through PEC by utilizing sunlight as the sole external energy input at zero external bias (0.0 V battery voltage) without any reduction in photocurrent. In PEC systems operating without external bias, water, oxygen, and sunlight alone are sufficient to achieve simultaneous wastewater purification and energy storage. This technology holds significant potential for advancements in both the environmental and energy sectors. Dong et al. [116] recently reported a groundbreaking study on a self-sustaining PEC system driven by solar energy without external biasing. The researchers successfully synthesized and utilized H_2O_2 *in situ* using synthetic leaf blades. Their findings indicated that by optimizing the coupling between the photoanode and cathode, they achieved an impressive unassisted production rate of H_2O_2 at 0.7 μmol min^{-1} cm^{-2}. This achievement represents an efficient self-circulating light Fenton-like system that solely relies on oxygen, water, and sunlight to accomplish wastewater treatment and energy storage objectives. The activation of O_2 by the PEF and PEC processes for organic pollutant degradation are summarized in Table 6.

4.3. Microbial fuel cell process

The MFC represents an innovative device that utilizes a microbial metabolic process to convert organic waste and various biomass into electrical energy [117,118]. In this metabolic process, microorganisms facilitate the conversion of organic substrates into electrical energy. Traditionally, an MFC consists of two electrodes (anode and cathode), separated by an electrolytic medium (Fig. 3d). Microorganisms thrive on the anode's surface and engage in respiration utilizing organic compounds, generating electrons and protons. Electrons flow through an external circuit toward the cathode, where O_2 undergoes a two-electron reduction, leading to H_2O_2 formation. The anaerobic exoelectrogenic bacteria in the anodic chamber of the MFC are capable of extracellular electron transfer [119], commonly known as "exoelectrogens" or "electrogens," including sulfate-reducing bacteria such as *Pseudomonas aeruginosa*, *Shewanella oneidensis*, and *E. coli*, among others [120]. These microorganisms significantly influence the oxygen reduction potential in an MFC.

An investigation focused on utilizing an MFC with graphite felt as an electrode and *S. oneidensis* MR-1 as the electroactive bacterium [121]. The MFC generated electricity *in situ* beneath the composite cathode, resulting in a peak H_2O_2 production of 135.9 mol L^{-1}, which subsequently reacted with leached Fe^{2+} to produce H_2O_2. At the same time, the system demonstrated a degradation efficiency of 78.3% toward triphenyltin chloride (TPTC). The presence of abundant microorganisms in the activated sludge effectively facilitated O_2 reduction. Soltani et al. [122] employed mixed active microorganisms collected from anaerobic digestion tanks in wastewater treatment plants as inoculum, using glucose as the carbon substrate. The findings revealed that after 8 h, the H_2O_2 concentration within the system reached 3.2 mg L^{-1}.

The electrode serves as a crucial site for microbial growth and adherence. The choice of electrode material significantly impacts the reduction of O_2 and the attenuation of pollutants. Wang et al. [123] developed an MFC utilizing acetylene black as the catalyst for H_2O_2 generation and Fe-Mn binary oxide as the catalyst for •OH generation. Compared to the EF process, the MFC exhibited a 38.0% increase in the CBZ elimination rate over 24 h. Rafaqat et al. [124] proposed a low-cost composite cathode composed of activated carbon/stainless steel (AC/SS) and graphite powder/stainless steel (GP/SS), where SS facilitated current distribution while AC/GP supported simultaneous H_2O_2 production. These dual-cathode variants achieved concurrent H_2O_2 generation at 1420.0 μM/2680.0 μM and an enhanced degradation rate for AR 114 of 96.0%/90.0%. Furthermore, the influence of factors such as proton exchange membranes, co-substrate diversity, MFC architecture, and hydraulic retention duration on *in situ* H_2O_2 synthesis within an MFC was uncovered. An MFC based on activated oxygen presents an economically viable and environmentally friendly technology for wastewater remediation and energy generation. However, the widespread implementation of MFCs faces challenges, including reduced current density, suboptimal conductivity, and inadequate H_2O_2 yield.

In summary, the newly developed methodologies for electrochemical oxygen activation exhibit significant advantages in pollutant remediation while also presenting technical and environmental challenges. The utilization of the Fenton reaction not only provides economic benefits but also reduces hazards associated with the handling, transportation, and containment of H_2O_2. Moreover, it effectively degrades pollutants by generating highly reactive •OH. However, practical implementation is hindered by high energy consumption and the requirement for supporting electrolytes. Additionally, the PEF process combines photocatalysis and electrocatalysis to enhance O_2 activation, resulting in increased production of ROS and improved capacity for pollutant removal. Nevertheless, this method necessitates simultaneous consumption of light and electrical energy and strict criteria for selecting the photocathode. The PEC process initiates O_2 activation through energy transfer and charge transfer processes. The efficiency of the entire process is determined by the choice of photoanode material, which presents a challenge in developing cost-effective and high-performing alternatives. MFC technology offers an economically and environmentally friendly approach by generating H_2O_2 within the cathode compartment, thereby reducing operational costs for wastewater treatment. MFCs utilize microorganisms to convert the chemical energy of organic compounds into electrical energy, representing a promising renewable energy technology. However, this technology faces limitations such as suboptimal H_2O_2 yield, diminished unit throughput, reduced current density, and inadequate conductivity. This investigation highlights that the efficacy of electrochemical activation processes heavily relies on acidic

Table 6
The activation of O_2 by photoelectro-Fenton process and photoelectrocatalytic process.

Cathodes	Anodes	Contaminants	Reaction conditions	O_2 supply	ROS	Removal efficiency	TOC removal	Reference
Carbon felt	Pt	CIP	$[CIP]_0 = 50.0$ mg L^{-1}, pH = 3.0, $Na_2SO_4 = 50.0$ μM, 300 W xenon lamp	O_2 aeration	H_2O_2, $\bullet O_2^-$, •OH	100.0%	80.3%	[98]
CP@pTTh	Zn foil	RhB	$[RhB]_0 = 16.0$ mg L^{-1}, pH = 3.0, $Na_2SO_4 = 50.0$ μM, j = 195.0 mA cm^{-2}, 300 W xenon lamp	O_2 aeration	H_2O_2, $\bullet O_2^-$, •OH	Almost 100.0%	-	[99]
FeCu@PC	RuO_2	SMT	$[SMT]_0 = 80.0$ mg L^{-1}, pH = 3.0–7.0, $Na_2SO_4 = 20.0$ mmol L^{-1}, I = 25.0 mA, 5 W UV lamp	O_2 aeration	H_2O_2, $\bullet O_2^-$, •OH	96.3%	73.3%	[100]
Co-free MWCNTs	BDD	Bronopol	$[Bronopol]_0 = 0.28$ mM, pH = 3.0, $Na_2SO = 50.0$ μM, Sunlight, j = 40.0 mA cm^{-2}	O_2 aeration	H_2O_2, •OH	94.0%	88.0%	[101]
GDE	Pt	SY dye	$[SY\ dye]_0 = 100.0$ mg L^{-1}, pH = 3.0, $Na_2SO_4 = 100.0$ mM, pH = 3.0, Solar irradiation, I = 100.0 mA	O_2 aeration	H_2O_2, •OH	100.0%	71.0%	[102]
GDE	BDD thin film	MET	$[MET]_0 = 90.0$ mg L^{-1}, pH = 3.0, $Na_2SO_4 = 50.0$ mM, j = 100.0 mA cm^{-2}	Air aeration	H_2O_2, •OH, $^1O_2$	70.0%	32.0%	[103]
FPC	WO_3	BPA	$[BPA]_0 = 10.0$ mg L^{-1}, pH = 3.0, $Na_2SO_4 = 50.0$ μM, 500 W xenon lamp, j = 1.0 mA cm^{-2}	O_2 aeration	H_2O_2, •OH	90.0%	40.0%	[107]
Carbon cloth	Fe_3O_4@$NiCo_2O_4$	RhB	$[RhB]_0 = 10.0$ mg L^{-1}, pH = 3.0, $Na_2SO_4 = 0.1$ M, j = 7.5 mA cm^{-2}, 150 W SAIC visible light lamp	O_2 aeration	H_2O_2, •OH	99.0%	60.0%	[108]
Pt	FST	SMT	$[SMT]_0 = 10.0$ mg L^{-1}, Acidic condition, $Na_2SO_4 = 0.1$ M, j = 7.7 mA cm^{-2}, LED light	Air aeration	H_2O_2, $\bullet O_2^-$, •OH	96.3%	73.3%	[112]
Mo-SACs/mrG	$SnO_{2-x}/BiVO_4$	MB	$[MB]_0 = 5.0$ mg L^{-1}, Acidic condition, Simulated solar light, j = 1.5 mA cm^{-2}	O_2 aeration	H_2O_2, •OH	99.5%	-	[116]

Abbreviations: CP@pTTh, carbon paper@polyterthiophene; FeCu@PC, FeCu@porous carbon; MWCNTs, multiwalled carbon nanotubes; BDD, boron-doped diamond; GDE, gas diffusion electrode; FPC, F-doped porous carbon; Mo-SACs/mrG, Mo single-atom catalysts/mildly reduced graphene; FST, Fe_3O_4@SiO_2@mesoporous TiO_2; CIP, ciprofloxacin; RhB, rhodamine B; SMT, sulfamethazine; SY, sunset yellow; MET, methomyl; BPA, bisphenol A; MB, methylene blue.

environments and access to pure oxygen (refer to Tables 5 and 6). Overcoming these challenges becomes crucial for advancing electrochemical oxygen activation.

5. Influencing factors of O_2 activation

The efficacy of O_2 activation methodologies relies on various factors, including the availability of O_2, reaction temperature, and pH level. Therefore, it is crucial to systematically optimize these parameters to enhance the efficiency of O_2 activation, improve pollutant removal capabilities, and establish a foundation for reducing operational expenditures.

5.1. Oxygen supply

Among the O_2 activation methods discussed in this paper, three types of O_2 supply are identified: air aeration, pure oxygen aeration, and dissolved oxygen in the solution itself. Based on the data presented in Tables 1 and it has been found that the primary source of O_2 during photocatalytic oxygen activation is the dissolved oxygen in the solution. These findings suggest these systems have demonstrated effective O_2 activation capabilities even under lower O_2 concentrations. This enhanced efficiency can be attributed to various modification strategies, such as defect engineering, doping, surface engineering, and ultrathin structures, which enhance the adsorption capacity of O_2.

Most studies in Tables 2 and 3 exhibit the use of air or pure oxygen aeration to activate O_2, indicating potential limitations in the efficacy of ZVMs and LVTMs for oxygen utilization. This may require high concentrations to activate O_2 and generate ROS, possibly due to the low adsorption capacity of ZVMs and LVTMs toward oxygen. The analysis in Table 4 reveals that dissolved oxygen is the primary source for activating O_2 through defect engineering, highlighting the crucial role of defect sites with a strong adsorptive propensity for O_2. Tables 5 and 6 further reveal that pure oxygen aeration is the principal method for the electrochemical activation of O_2, where purity significantly impacts H_2O_2 generation. However, the practical implementation of pollution control measures favors alternative approaches over pure oxygen aeration due to suboptimal oxygen utilization and substantial energy consumption losses, posing challenges for large-scale adoption.

During the aeration process, bubbles' size plays a crucial role in activating O_2. Microbubbles (MBs) and nanobubbles (NBs), with their larger surface areas compared to large bubbles, facilitate faster diffusion rates of O_2 and longer hydraulic retention times [125,126]. Consequently, MBs and NBs can effectively provide water with a sustained oxygen supply. It is worth noting that MBs and NBs release a substantial amount of energy upon collapse, generating ROS [127]. For instance, Ghadimkhani et al. [128] elucidated that when NBs burst into molecular gas, they liberate considerable surface energy capable of converting O_2 into radicals.

In conclusion, air aeration, pure oxygen aeration, and dissolved oxygen within solutions are vital sources in activation systems that significantly contribute to the degradation of pollutants through ROS. Additionally, oxygenation efficiency and pollutant removal are profoundly influenced by the size of gas bubbles. Therefore, it is imperative to carefully select an appropriate method for supplying oxygen based on the specific requirements and specifications of the processing system.

5.2. Reaction temperature

As an important experimental parameter, reaction temperature significantly impacts O_2 activation. Typically, oxygen activation processes occur in ambient room temperature conditions. The reaction temperature has a bidirectional effect on both O_2 activation and the generation of ROS. Temperature increases can enhance pollutant mass transfer capacity and O_2 diffusion [129]. However, excessively high temperatures decrease O_2 solubility and accelerate the H_2O_2 self-decomposition rate [130].

5.3. pH

The pH level plays a crucial role in the activation of O_2. As shown in Table 1, the photochemical activation of O_2 is feasible under both acidic and marginally alkaline conditions. In contrast to acidic

environments, alkaline settings can significantly reduce the oxidation efficiency of pollutants. Under strongly alkaline conditions, semiconductor material surfaces may become negatively charged, attracting holes and repelling electrons, thereby influencing their recombination at the surface. This phenomenon hinders the formation of ROS, ultimately resulting in a diminished capacity for pollutant degradation [131]. Table 1 demonstrates that mild alkaline conditions promote pollutant degradation, which may be attributed to the dissociation constant (pKa) of the pollutants. However, when the pH exceeds the pKa value of the pollutants, an excess of OH^- can induce electrostatic repulsion between pollutant anions and the negatively charged catalyst surface, impeding pollutant degradation efficiency [132].

The chemical activation of O_2 predominantly occurs in both acidic and marginally alkaline environments, providing informative background information (Tables 2–4). It is well-known that acidic conditions are favorable for pollutant degradation due to the corrosion of zero-valent metals, which initiates the activation of O_2. Under acidic conditions, a lower pH facilitates the release of low-valent metal ions from zero-valent metals and the dissolution of oxide layers on their surfaces. However, it should be noted that excessively high pH levels impede the efficacy of pollutant degradation as metal ions quickly bind with OH^-, forming adverse metal hydroxide precipitates that hinder ROS generation [71]. Moreover, compared to alkaline milieus, acidic conditions significantly elevate the redox potential of $O_2/\bullet O_2^-$, thereby increasing its propensity for conversion into $\bullet O_2^-$ in the presence of acid [133]. The importance of pH is further highlighted by its facilitation of the *in situ* synthesis of H_2O_2 during reduction processes involving proton participation. Conversely, alkaline conditions favor H_2O_2 disintegration and mitigate catalyst deactivation phenomena. Nonetheless, an overly diminished pH level within the solution may lead to alternative reactions and concurrently impact catalyst stability.

An acidic environment is essential for the optimal efficacy of the electrochemical activation process of O_2 (Tables 5 and 6). During this process, H_2O_2 serves as the main ROS generated. The production of H_2O_2 relies on the presence of $\bullet O_2^-$, a pair of protons, and a single electron. In an alkaline milieu, an abundance of OH^- persistently consumes protons, thereby hindering the formation of H_2O_2. However, excessively low pH levels impede the interaction between metal ions and H_2O_2, reducing diminished •OH production.

6. ROS generation path based on O_2 activation

O_2, known for its safety, environmental friendliness, and green properties, exists in the stable triplet oxygen ($^3O_2$) with two unpaired electrons in its highest occupied molecular orbital (HOMO). The activation of O_2 involves the acquisition of electrons and energy, which weakens the oxygen–oxygen bond and leads to the generation of ROS [134]. This study elucidates three fundamental approaches for activating O_2: photocatalytic, chemical, and electrochemical methods. This article provides a comprehensive summary and analysis of each ROS production pathway, contributing to a better understanding of strategies for activating O_2.

$\bullet O_2^-$ is an important ROS involved in the mineralization of organic molecules and serves as an intermediate in the generation of other ROS. The predominant source of $\bullet O_2^-$ production is through the single-electron reduction of O_2, although the electron donor for this reduction varies depending on different activation strategies. In photochemical activation processes, O_2 is activated by photo-excited electrons in a semiconductor; however, the reduction of O_2 to $\bullet O_2^-$ via photo-generated electrons requires that the semiconductor's conduction band potential be lower than the standard redox potential of $O_2/\bullet O_2^-$ ($E = -0.05$ eV vs. normal hydrogen electrode (NHE)) [135]. Additionally, valence band holes can oxidize H_2O_2 and generate $\bullet O_2^-$. In chemical activation processes, electron donors such as ZVMs, LVTMs, and materials with defect engineering reduce O_2. ZVMs and LVTMs possess good reducibility because they can easily donate one or multiple electrons. Moreover, defect engineering involving OVs provides an abundance of electrons capable of reducing O_2, forming $\bullet O_2^-$. Unlike ZVMs and LVTMs, OVs can induce the adsorption and interaction of O_2 in their vicinity, influenced by localized charge effects, reduced surface energy, and other contributing factors. O_2 is sequestered at these OVs, leading to elongation of the O–O bond within the oxygen molecule toward its theoretical length of $\bullet O_2^-$ (1.26 Å) [80]. This elongation occurs as electrons are transferred from the OVs to the $\pi 2py^*$ orbital of O_2, ultimately resulting in the formation of $\bullet O_2^-$. During electrochemical activation, O_2 can acquire electrons on the photoanode and cathode, thereby undergoing reduction to form $\bullet O_2^-$.

The *in situ* production of H_2O_2 plays a crucial role in the degradation process of organic pollutants. This is primarily achieved through oxygen reduction by photo-generated electrons, metals, defects, and the cathode surface. In photochemical processes, semiconductors can generate photoelectrons that reduce O_2 to produce H_2O_2. There are two distinct pathways for the reduction of O_2 to H_2O_2: the first entails a direct two-electron reduction (equation (22)), while the second involves a one-electron, two-stage indirect reduction sequence (equations (23) and (24)). O_2 can directly gain two electrons and two protons to form H_2O_2. Additionally, O_2 initially undergoes a reaction to yield $\bullet O_2^-$ by accepting a single electron before assimilating an additional electron and two protons to form H_2O_2.

$$O_2 + 2H^+ + 2e^- \rightarrow H_2O_2 \tag{22}$$

$$O_2 + e^- \rightarrow \bullet O_2^- \tag{23}$$

$$\bullet O_2^- + 2H^+ + e^- \rightarrow H_2O_2 \tag{24}$$

The band structure is critical to distinguishing between the two activation pathways. Considering that the standard potential for the two-electron transfer process is 0.68 V vs. NHE [136], O_2 activation can occur through a one-step two-electron transfer process if the catalyst's conduction band potential is below this threshold. Additionally, in the two-step single-electron transfer of O_2, $\bullet O_2^-$ acts as an intermediate species; therefore, introducing an $\bullet O_2^-$ scavenger can inhibit the single-electron transfer sequence. If introducing a scavenger leads to no formation of H_2O_2, it indicates that H_2O_2 synthesis exclusively occurs via the single-electron transfer pathway of O_2. However, ORRs do not always result in H_2O_2 formation. O_2 undergoes a four-electron reduction process at excessively high voltages, producing H_2O.

The •OH radical, known for its exceptional oxidative properties in eliminating organic pollutants, is formed through the reduction and hydrogenation of O_2 to $\bullet O_2^-$, followed by a subsequent conversion into H_2O_2 with a lower energy barrier. This electron reduction process facilitates a more favorable reaction pathway, leading to the subsequent reduction of H_2O_2 to •OH. Moreover, photo-induced holes in semiconductors can generate •OH through oxidation when the valence band position of the semiconductor aligns with the required standard potential (equation (25)).

$$H_2O + h^+ \rightarrow \bullet OH + H^+ \tag{25}$$

O_2 exists in three electron configurations: two low-lying singlet excited states ($O_2(1\Delta g)$ and $O_2(1\Sigma g^+)$) and a ground state triplet ($O_2(3\Sigma g^-)$) [137]. Since the energies of $O_2(1\Delta g)$ (95.0 kJ mol^{-1}) and $O_2(1\Sigma g^+)$ (158.0 kJ mol^{-1}) are higher than the ground state triplet,

singlet excited states exhibit higher reactivity. When the spin restriction of $^3O_2$ is overcome, electrons join one of the orbitals to form "singlet oxygen delta" $O_2(1\Delta g)$, a rare chemical species with high chemical reactivity [138]. The transition from the $1\Delta g$ state to the $3\Sigma g^-$ state is spin-forbidden, making $O_2(1\Delta g)$ a relatively long-lived species. $O_2(1\Sigma g^+)$, on the other hand, has a shorter lifespan due to the allowed spin transition to the $O_2(1\Delta g)$ state, so the term "singlet oxygen" mainly refers to $O_2(1\Delta g)$ [139].

Based on the activation of O_2, the generation pathways of $^1O_2$ can be broadly categorized into electron transfer and energy transfer (refer to Tables 1 and 6). In the electron transfer process, $^1O_2$ can be produced through the redox reactions involving O_2 or radicals. Although H_2O_2 is capable of generating $^1O_2$ through self-decomposition, this sequence occurs at a relatively slow rate. $\bullet O_2^-$ plays a crucial role as an intermediate species generating of $^1O_2$. Potent oxidants possess the ability to directly convert $\bullet O_2^-$ into $^1O_2$. Photo-generated holcan to interact with $\bullet O_2^-$ leading to the formation $^1O_2$. The oxidative processes involving radicals such as $\bullet OH$ and $\bullet OOH$ further facilitate the conversion of $\bullet O_2^-$ into $^1O_2$. Additionally, high-valence metal ions have a propensity for oxidizing $\bullet O_2^-$. These reactions can be observed in the photochemical, chemical, and electrochemical activation of O_2 (equations (26)–(29)).

$$O_2 + e^- \rightarrow \bullet O_2^- \tag{26}$$

$$\bullet O_2^- + h^+ \rightarrow {}^1O_2 \tag{27}$$

$$\bullet O_2^- + 2\bullet OH + 2H^+ \rightarrow {}^1O_2 + 2OH^- \tag{28}$$

$$\bullet O_2^- + Co^{4+} \big/ Co^{3+} \rightarrow {}^1O_2 + 2Co^{2+} \tag{29}$$

The transformation of O_2 into $^1O_2$ via energy transfer is currently limited to photochemical O_2 activation. In its ground state, the oxygen molecule exists as $^3O_2$, with the spins of its two unpaired electrons parallel [140]. When the spin states of these electrons change to become antiparallel, the oxygen molecule converts into $^1O_2$. Under illumination, semiconductor photocatalysts generate excitons, electron-hole pairs induced by photon absorption. Before exciton–exciton annihilation (EEA), singlet excitons undergo intersystem crossing (ISC) and transition to energetically favorable triplet states [141]. This process involves a change in electron spin orientation, resulting in the formation of long-lived triplet excitons. The triplet excitons transfer energy to O_2, inducing a spin state change (spin flip) that generates $^1O_2$ (Fig. 4). $^1O_2$ is a high-energy form of oxygen with strong oxidizing power, enabling its involvement in diverse chemical reactions, including the oxidation of organic compounds.

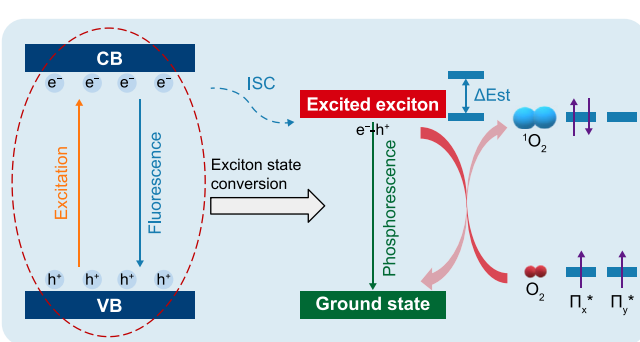

Fig. 4. The production mechanism of $^1O_2$ by O_2 activation through energy transfer.

7. Conclusions and outlook

O_2, known for its environmentally friendly, non-toxic, and cost-effective properties, stands out as a superior oxidant in the sustainable degradation of contaminants. The activation of O_2 leads to the generation of ROS, which are instrumental in efficiently degrading and mineralizing various organic pollutants. This study presents a comprehensive analysis of recent advancements in utilizing oxygen as an oxidant for environmental remediation. Several strategies have been developed to activate O_2, including photochemical, chemical, and electrochemical methods. These approaches have shown remarkable outcomes in wastewater treatment. Notably, energy and electron transfer are the primary mechanisms underlying O_2 activation. Given its paramount importance in environmental remediation, there is significant interest among researchers regarding the activation of O_2. However, this field is still at an early stage, with numerous complexities and challenges that have yet to be addressed. Therefore, meticulous research is essential to provide valuable theoretical references for future investigations.

First, it is crucial to minimize energy consumption in applications to achieve energy-efficient and environmentally benign water purification technologies. The electrochemical activation process using pure oxygen aeration may have low oxygen utilization efficiency and high energy consumption. Therefore, exploring the use of ambient air or oxygen generated via water electrolysis as alternatives for the reaction becomes essential to address this research gap. Simultaneously, transitioning toward low-power light sources or solar energy should be considered wherever feasible for photochemical activation.

Second, intensifying research efforts on the selective generation of $^1O_2$ is pivotal. $^1O_2$ stands out due to its extended lifespan and selectivity as the sole ROS producible via both energy transfer and electron transfer mechanisms. Optimizing the activation process to enhance $^1O_2$ yield is important while conducting comprehensive studies elucidating the underlying formation mechanisms during O_2 activation.

Moreover, comprehensive investigations are warranted to unravel the intricate activation mechanism of O_2 within complex aquatic ecosystems. Rigorous experimental studies are essential for unveiling the nuanced complexities of O_2 activation, aiming to achieve targeted pollutant removal and efficient resource utilization.

Ultimately, a versatile wastewater treatment system can be structured by synergizing diverse activation methods and leveraging their strengths. For instance, by synergistically integrating photocatalytic and electrocatalytic technologies, solar energy can be harnessed while concurrently regulating reactions via electricity, thereby amplifying the efficiency of the treatment process.

CRediT authorship contribution statement

Xiaohu Fan: Writing - Original Draft, Visualization, Software, Methodology, Investigation, Data Curation. **Qiang Fu:** Methodology, Investigation. **Guorui Liu:** Methodology, Investigation. **Hongliang Jia:** Methodology, Conceptualization. **Xiaolong Dong:** Visualization. **Yi-Fan Li:** Methodology, Formal Analysis. **Song Cui:** Writing - Review & Editing, Validation, Supervision, Resources, Methodology, Funding Acquisition, Conceptualization.

Declaration of competing interest

The authors declare that they have no known competing financial interests or personal relationships that could have

appeared to influence the work reported in this paper.

Acknowledgments

This work was supported by the Distinguished Youth Science Foundation of Heilongjiang Province, China (JQ2023E001) and Young Leading Talents of Northeast Agricultural University, China (NEAU2023QNLJ-013).

References

[1] P. Liu, J. Dai, C. Bie, H. Li, Z. Zhang, X. Guo, L. Zhu, Bioaccessibility of microplastic-associated antibiotics in freshwater organisms: highlighting the impacts of biofilm colonization via an in vitro protocol, Environ. Sci. Technol. 56 (17) (2022) 12267–12277, https://doi.org/10.1021/acs.est.2c02782.

[2] M. Khmaissa, H. Zouari-Mechichi, G. Sciara, E. Record, T. Mechichi, Pollution from livestock farming antibiotics an emerging environmental and human health concern: a review, J. Hazard Mater. 13 (2024) 100410, https://doi.org/10.1016/j.hazadv.2024.100410.

[3] K.J. Harris, G. Munoz, V. Woo, S. Sauve, A.A. Rand, Targeted and suspect screening of per- and polyfluoroalkyl substances in cosmetics and personal care products, Environ. Sci. Technol. 56 (20) (2022) 14594–14604, https://doi.org/10.1021/acs.est.2c02660.

[4] A. Mukherjee, A. Mullick, P. Vadthya, S. Moulik, A. Roy, Surfactant degradation using hydrodynamic cavitation based hybrid advanced oxidation technology: a techno economic feasibility study, Chem. Eng. J. 398 (2020) 125599, https://doi.org/10.1016/j.cej.2020.125599.

[5] T. Xia, Y. Lin, W. Li, M. Ju, Photocatalytic degradation of organic pollutants by MOFs based materials: a review, Chin. Chem. Lett. 32 (10) (2021) 2975–2984, https://doi.org/10.1016/j.cclet.2021.02.058.

[6] Z.H. Xie, C.S. He, D.N. Pei, Y. Dong, S.R. Yang, Z. Xiong, P. Zhou, Z.C. Pan, G. Yao, B. Lai, Review of characteristics, generation pathways and detection methods of singlet oxygen generated in advanced oxidation processes (AOPs), Chem. Eng. J. 468 (2023) 143778, https://doi.org/10.1016/j.cej.2023.143778.

[7] H. Yan, C. Lai, S. Liu, D. Wang, X. Zhou, M. Zhang, L. Li, D. Ma, F. Xu, X. Huo, L. Tang, M. Yan, J. Nie, X. Fan, Insight into the selective oxidation behavior of organic pollutants via Ni-N_4-C mediated electron transfer pathway, Chem. Eng. J. 473 (2023) 145253, https://doi.org/10.1016/j.cej.2023.145253.

[8] S. Giannakis, K.-Y.A. Lin, F. Ghanbari, A review of the recent advances on the treatment of industrial wastewaters by Sulfate Radical-based Advanced Oxidation Processes (SR-AOPs), Chem. Eng. J. 406 (2021) 127083, https://doi.org/10.1016/j.cej.2020.127083.

[9] S. Akbari, G. Moussavi, J. Decker, M.L. Marin, F. Bosca, S. Giannakis, Superior visible light-mediated catalytic activity of a novel N-doped, Fe_3O_4-incorporating MgO nanosheet in presence of PMS: imidacloprid degradation and implications on simultaneous bacterial inactivation, Appl. Catal. B Environ. 317 (2022) 121732, https://doi.org/10.1016/j.apcatb.2022.121732.

[10] J. Qin, Z. Liu, W. Xu, X. Zhu, F. Liang, Y. Yu, Y. Zheng, L. Yao, H. Zhang, K. Lin, J. Fang, Z. Fang, Heterogeneous photocatalysis coupled with Fenton-Like reaction for fluoroquinolone antibiotics degradation by poly (Triazine Imide): from mechanism to application in a continuous flow catalytic system, Chem. Eng. J. 476 (2023) 146856, https://doi.org/10.1016/j.cej.2023.146856.

[11] B.G. Fu, X. Zhou, Y. Lu, W.Z. Quan, C. Li, L. Cheng, X. Xiao, Y.Y. Yu, Interfacial OOH* mediated Fe(II) regeneration on the single atom Co-N-C catalyst for efficient Fenton-like processes, J. Hazard Mater. (2024) 134214, https://doi.org/10.1016/j.jhazmat.2024.134214.

[12] W. Feng, Y. Jiang, F. Ge, Q. Bai, J. Yang, L. Shang, R. Cao, G. Niu, L. Wang, Z. Zhu, N. Sui, Interconversion of sp-hybridized chemical bonds induces piezoelectric enhanced photocatalysis, Appl. Catal. B Environ. 349 (2024) 123868, https://doi.org/10.1016/j.apcatb.2024.123868.

[13] S. Yang, Y. Feng, D. Gao, X. Wang, N. Suo, Y. Yu, S. Zhang, Electrocatalysis degradation of tetracycline in a three-dimensional aeration electrocatalysis reactor (3D-AER) with a flotation-tailings particle electrode (FPE): physicochemical properties, influencing factors and the degradation mechanism, J. Hazard Mater. 407 (2021) 124361, https://doi.org/10.1016/j.jhazmat.2020.124361.

[14] H. Wang, Z. Long, R. Chen, H. Zhang, H. Shi, Y. Chen, Boosting PMS activation over BiVO4 piezo-photocatalyst to rapidly degrade tetracycline: intermediates and mechanism, Sep. Purif. Technol. 331 (2024) 125598, https://doi.org/10.1016/j.seppur.2023.125598.

[15] Z.T. Dong, C.G. Niu, H. Guo, H.Y. Niu, S. Liang, C. Liang, H.Y. Liu, Y.Y. Yang, Anchoring CuFe2O4 nanoparticles into N-doped carbon nanosheets for peroxymonosulfate activation: built-in electric field dominated radical and non-radical process, Chem. Eng. J. 426 (2021) 130850, https://doi.org/10.1016/j.cej.2021.130850.

[16] C. Lai, H. Yan, D. Wang, S. Liu, X. Zhou, X. Li, M. Zhang, L. Li, Y. Fu, F. Xu, X. Yang, X. Huo, Facile synthesis of Mn, Ce co-doped g-C_3N_4 composite for peroxymonosulfate activation towards organic contaminant degradation, Chemosphere 293 (2022) 133472, https://doi.org/10.1016/j.chemosphere.2021.133472.

[17] H. Zhou, J. Yang, W. Cao, C. Chen, C. Jiang, Y. Wang, Hollow Meso-crystalline Mn-doped Fe_3O_4 Fenton-like catalysis for ciprofloxacin degradation: applications in water purification on wide pH range, Appl. Surf. Sci. 590 (2022) 153120, https://doi.org/10.1016/j.apsusc.2022.153120.

[18] Q. Yi, J. Ji, B. Shen, C. Dong, J. Liu, J. Zhang, M. Xing, Singlet Oxygen triggered by superoxide radicals in a molybdenum cocatalytic Fenton reaction with enhanced redox activity in the environment, Environ. Sci. Technol. 53 (16) (2019) 9725–9733, https://doi.org/10.1021/acs.est.9b01676.

[19] Y. Xu, M. Guo, C. Ge, P. Zhang, W. Xu, L. Zhang, S. Zhou, J. Liao, Cu single atoms/O doping g-C_3N_4 mediated photocatalytic activation of peroxymonosulfate for ultrafast carbamazepine removal via high $^1O_2$ yield, Appl. Surf. Sci. 640 (2023) 158290, https://doi.org/10.1016/j.apsusc.2023.158290.

[20] H. Sun, P. Qin, J. Guo, Y. Jiang, Y. Liang, X. Gong, X. Ma, Q. Wu, J. Zhang, L. Luo, Z. Wu, Enhanced electron channel via the interfacial heterotropic electric field in dual S-scheme g-C_3N_4/WO_3/ZnS photocatalyst for year-round antibiotic degradation under sunlight, Chem. Eng. J. 470 (2023) 144217, https://doi.org/10.1016/j.cej.2023.144217.

[21] P. Lyu, J. Zhu, C. Han, L. Qiang, L. Zhang, B. Mei, J. He, X. Liu, Z. Bian, H. Li, Self-driven reactive oxygen species generation via interfacial oxygen vacancies on carbon-coated TiO_{2-x} with versatile applications, ACS Appl. Mater. Interfaces 13 (1) (2021) 2033–2043, https://doi.org/10.1021/acsami.0c19414.

[22] X. Sun, X. Luo, X. Zhang, J. Xie, S. Jin, H. Wang, X. Zheng, X. Wu, Y. Xie, Enhanced superoxide generation on defective surfaces for selective photooxidation, J. Am. Chem. Soc. 141 (9) (2019) 3797–3801, https://doi.org/10.1021/jacs.8b13051.

[23] H. Zhao, X. Liu, Y. Dong, Y. Xia, H. Wang, A special synthesis of BiOCl photocatalyst for efficient pollutants removal: new insight into the band structure regulation and molecular oxygen activation, Appl. Catal. B Environ. 256 (2019) 117872, https://doi.org/10.1016/j.apcatb.2019.117872.

[24] S. Wang, Z. Xiong, N. Yang, X. Ding, H. Chen, Iodine-doping-assisted tunable introduction of oxygen vacancies on bismuth tungstate photocatalysts for highly efficient molecular oxygen activation and pentachlorophenol mineralization, Chin. J. Catal. 41 (10) (2020) 1544–1553, https://doi.org/10.1016/S1872-2067(19)63506-0.

[25] Q. Wang, D. Xu, Y. Dong, S. Pang, L. Zhang, G. Zhang, L. Lv, X. Liu, Y. Xia, L.C. Campos, Z. Ren, P. Wang, Unsaturated Nd-Bi dual-metal sites enable efficient NIR light-driven O_2 activation for water purification, Appl. Catal. B Environ. 319 (2022) 121924, https://doi.org/10.1016/j.apcatb.2022.121924.

[26] J. Sheng, X. Li, Y. Xu, Generation of H_2O_2 and OH radicals on Bi_2WO_6 for phenol degradation under visible light, ACS Catal. 4 (3) (2014) 732–737, https://doi.org/10.1021/cs400927w.

[27] H. Liu, C. Wang, Y. Yang, M. Gao, A. Xue, H. Chen, X. Ding, Selective photocatalytic remediation of para-substituted phenol pollutants over iodine-doped Bi_2MoO_6 via in-situ generated H_2O_2 and iodine radicals activation, Sep. Purif. Technol. 340 (2024) 126711, https://doi.org/10.1016/j.seppur.2024.126711.

[28] C. Yue, N. Sun, Y. Qiu, L. Zhu, Z. Du, F. Liu, A direct Z-scheme 0D α-Fe_2O_3/TiO_2 heterojunction for enhanced photo-Fenton activity with low H_2O_2 consumption, Chin. Chem. Lett. (2024) 109698, https://doi.org/10.1016/j.cclet.2024.109698.

[29] L.W. Wei, M.W. Zheng, S.H. Liu, H. Paul Wang, Y.C. Pu, V.C. Nguyen, Visible-light photocatalytic O_2-to-H_2O_2 via nitrogen-graphene quantum dots-modified $Bi_2Fe_4O_9$ for synchronizing the reduction of Cr(VI) and oxidation of organic contaminants: kinetics, mechanism, and performance, Chem. Eng. J. 487 (2024) 150712, https://doi.org/10.1016/j.cej.2024.150712.

[30] H. Sun, P. Qin, J. Guo, Y. Jiang, Y. Liang, X. Gong, X. Ma, Q. Wu, J. Zhang, L. Luo, Z. Wu, Enhanced electron channel via the interfacial heterotropic electric field in dual S-scheme g-C_3N_4/WO_3/ZnS photocatalyst for year-round antibiotic degradation under sunlight, Chem. Eng. J. 470 (2023) 144217, https://doi.org/10.1016/j.cej.2023.144217.

[31] W. Liu, P. Wang, J. Chen, X. Gao, H. Che, X. Su, B. Liu, Y. Ao, In situ single iron atom doping on Bi_2WO_6 monolayers triggers efficient photo-fenton reaction, Environ. Sci. Ecotechnol. (2024) 100414, https://doi.org/10.1016/j.ese.2024.100414.

[32] Z. Yang, J. Wang, Photo-Fenton degradation of sulfamethazine using self-assembled CdS nanorods with in-situ production of H_2O_2 at wide pH range, Chem. Eng. J. 450 (2022) 138024, https://doi.org/10.1016/j.cej.2022.138024.

[33] Z. Jiang, L. Wang, J. Lei, Y. Liu, J. Zhang, Photo-Fenton degradation of phenol by CdS/rGO/Fe^{2+} at natural pH with in situ-generated H_2O_2, Appl. Catal. B Environ. 241 (2019) 367–374, https://doi.org/10.1016/j.apcatb.2018.09.049.

[34] W. Shi, L. Wang, J. Wang, H. Sun, Y. Shi, F. Guo, C. Lu, Magnetically retrievable CdS/reduced graphene oxide/$ZnFe_2O_4$ ternary nanocomposite for self-generated H_2O_2 towards photo-Fenton removal of tetracycline under visible light irradiation, Sep. Purif. Technol. 292 (2022) 120987, https://doi.org/10.1016/j.seppur.2022.120987.

[35] Y.Y. Yang, H. Guo, D.W. Huang, L. Li, H.Y. Liu, L. Sui, Q. Wu, J.J. Zhu, L. Zhang, C.G. Niu, Simultaneously tuning oxygen reduction pathway and charge transfer dynamics toward sacrificial agent-free photocatalytic H_2O_2 production for in-situ water disinfection, Chem. Eng. J. 479 (2024) 147863, https://doi.org/10.1016/j.cej.2023.147863.

[36] C. Du, W. Feng, S. Nie, X. Su, H. Liu, J. Feng, J. Sun, C. Hu, S. Dong, π-π conjugation driving degradation of aromatic compounds with in-situ hydrogen peroxide generation over $Zn_2In_2S_5$ grown on nitrogen-doped

carbon spheres, Appl. Catal. B Environ. 310 (2022) 121298, https://doi.org/10.1016/j.apcatb.2022.121298.
[37] M.A. Mushtaq, A. Kumar, G. Yasin, M. Arif, M. Tabish, S. Ibraheem, X. Cai, W. Ye, X. Fang, A. Saad, J. Zhao, S. Ji, D. Yan, 3D interconnected porous Mo-doped WO_3@CdS hierarchical hollow heterostructures for efficient photoelectrochemical nitrogen reduction to ammonia, Appl. Catal. B Environ. 317 (2022) 121711, https://doi.org/10.1016/j.apcatb.2022.121711.
[38] R.P. Gaikwad, D.R. Naikwadi, A.V. Biradar, M.B. Gawande, Photocatalytic one-pot conversion of aldehydes to esters and degradation of rhodamine B dye using mesoporous graphitic carbon nitride, ACS Appl. Nano Mater. 6 (3) (2023) 1859–1869, https://doi.org/10.1021/acsanm.2c04846.
[39] A.M. Chávez, A. Torres-Pinto, P.M. Álvarez, J.L. Faria, C.G. Silva, A.M.T. Silva, One-pot synthesis and immobilization of urea-derived graphitic carbon nitride onto ceramic foams for visible-light photocatalytic wet peroxide oxidation in water treatment, Chem. Eng. J. 481 (2024), https://doi.org/10.1016/j.cej.2023.148141.
[40] Y. Wu, J. Chen, H. Che, X. Gao, Y. Ao, P. Wang, Boosting $2e^-$ oxygen reduction reaction in garland carbon nitride with carbon defects for high-efficient photocatalysis-self-Fenton degradation of 2,4-dichlorophenol, Appl. Catal. B Environ. 307 (2022) 121185, https://doi.org/10.1016/j.apcatb.2022.121185.
[41] W.J. Ong, L.L. Tan, Y.H. Ng, S.T. Yong, S.P. Chai, Graphitic carbon nitride (g-C_3N_4)-based photocatalysts for artificial photosynthesis and environmental remediation: are we a step closer to achieving sustainability? Chem. Rev. 116 (12) (2016) 7159–7329, https://doi.org/10.1021/acs.chemrev.6b00075.
[42] H. Deng, Y. Jia, W. Wang, S. Zhong, R. Hao, L. Fan, X. Liu, Defect and crystallinity-mediated charge separation in carbon nitride for synergistically boosted solar-driven hydrogen evolution, ACS Sustain. Chem. Eng. 11 (37) (2023) 13736–13746, https://doi.org/10.1021/acssuschemeng.3c03772.
[43] N. Aquino de Carvalho, Y. Wang, N. Morales-Soto, D. Waldeck, K. Bibby, K. Doudrick, L.M. Gilbertson, Using C-doping to identify photocatalytic properties of graphitic carbon nitride that govern antibacterial efficacy, ACS ES&T Water 1 (2) (2020) 269–280, https://doi.org/10.1021/acsestwater.0c00053.
[44] M. Aggarwal, S. Basu, N.P. Shetti, M.N. Nadagouda, E.E. Kwon, Y.-K. Park, T.M. Aminabhavi, Photocatalytic carbon dioxide reduction: exploring the role of ultrathin 2D graphitic carbon nitride (g-C_3N_4), Chem. Eng. J. 425 (2021) 131402, https://doi.org/10.1016/j.cej.2021.131402.
[45] Q. Zhang, B. Wang, H. Miao, J. Fan, T. Sun, E. Liu, Efficient photocatalytic H_2O_2 production over K^+-intercalated crystalline g-C_3N_4 with regulated oxygen reduction pathway, Chem. Eng. J. 482 (2024) 148844, https://doi.org/10.1016/j.cej.2024.148844.
[46] Z. Zhou, K. Li, W. Deng, J. Li, Y. Yan, Y. Li, X. Quan, T. Wang, Nitrogen vacancy mediated exciton dissociation in carbon nitride nanosheets: enhanced hydroxyl radicals generation for efficient photocatalytic degradation of organic pollutants, J. Hazard Mater. 387 (2020) 122023, https://doi.org/10.1016/j.jhazmat.2020.122023.
[47] R. Li, M. Zheng, X. Zhou, D. Zhang, Y. Shi, C. Li, M. Yang, Carbon vacancies in porous g-C3N4 nanosheets induced robust H_2O_2 production for highly efficient photocatalysis-self-Fenton system for metronidazole degradation, Chem. Eng. J. 464 (2023) 142584, https://doi.org/10.1016/j.cej.2023.142584.
[48] J. Hu, P. Zhang, T. Yang, Y. Cai, J. Qu, X. Yang, Screen superior ultra-thin g-C_3N_4 material for photocatalytic in-situ H_2O_2 production to remove tetracycline, Appl. Surf. Sci. 576 (2022) 151841, https://doi.org/10.1016/j.apsusc.2021.151841.
[49] W. Shi, W. Sun, Y. Liu, K. Zhang, H. Sun, X. Lin, Y. Hong, F. Guo, A self-sufficient photo-Fenton system with coupling in-situ production H_2O_2 of ultrathin porous g-C_3N_4 nanosheets and amorphous FeOOH quantum dots, J. Hazard Mater. 436 (2022) 129141, https://doi.org/10.1016/j.jhazmat.2022.129141.
[50] J. Ma, K. Wang, C. Wang, X. Chen, W. Zhu, G. Zhu, W. Yao, Y. Zhu, Photocatalysis-self-Fenton system with high-fluent degradation and high mineralization ability, Appl. Catal. B Environ. 276 (2020) 119150, https://doi.org/10.1016/j.apcatb.2020.119150.
[51] Z. Wei, M. Liu, Z. Zhang, W. Yao, H. Tan, Y. Zhu, Efficient visible-light-driven selective oxygen reduction to hydrogen peroxide by oxygen-enriched graphitic carbon nitride polymers, Energy Environ. Sci. 11 (9) (2018) 2581–2589, https://doi.org/10.1039/C8EE01316K.
[52] L.L. Liu, F. Chen, J.H. Wu, J.J. Chen, H.Q. Yu, Synergy of crystallinity modulation and intercalation engineering in carbon nitride for boosted H_2O_2 photosynthesis, Proc. Natl. Acad. Sci. U. S. A. 120 (6) (2023) e2215305120, https://doi.org/10.1073/pnas.2215305120.
[53] C. Du, W. Feng, S. Nie, J. Zhang, Y. Liang, X. Han, Y. Wu, J. Feng, S. Dong, H. Liu, J. Sun, Harnessing efficient in-situ H_2O_2 production via a KPF_6/BiOBr photocatalyst for the degradation of polyethylene, Sep. Purif. Technol. 279 (2021) 119734, https://doi.org/10.1016/j.seppur.2021.119734.
[54] H. Wang, S. Jiang, S. Chen, D. Li, X. Zhang, W. Shao, X. Sun, J. Xie, Z. Zhao, Q. Zhang, Y. Tian, Y. Xie, Enhanced singlet oxygen generation in oxidized graphitic carbon nitride for organic synthesis, Adv. Mater. 28 (32) (2016) 6940–6945, https://doi.org/10.1002/adma.201601413.
[55] R. Yamaguchi, S. Kurosu, M. Suzuki, Y. Kawase, Hydroxyl radical generation by zero-valent iron/Cu (ZVI/Cu) bimetallic catalyst in wastewater treatment: heterogeneous Fenton/Fenton-like reactions by Fenton reagents formed in-situ under oxic conditions, Chem. Eng. J. 334 (2018) 1537–1549, https://doi.org/10.1016/j.cej.2017.10.154.
[56] C. Fan, S. Wu, X. Zheng, K. Bei, S. He, M. Zhao, Enhancement of cottonseed oil refining wastewater treatment by zero valent iron under sunlight irradiation and O_2 bubbling, J. Colloid Interface Sci. 615 (2022) 124–132, https://doi.org/10.1016/j.jcis.2022.01.171.
[57] H. Lv, H. Niu, X. Zhao, Y. Cai, F. Wu, Carbon zero-valent iron materials possessing high-content fine Fe^0 nanoparticles with enhanced microelectrolysis-Fenton-like catalytic performance for water purification, Appl. Catal. B Environ. 286 (2021) 119940, https://doi.org/10.1016/j.apcatb.2021.119940.
[58] Y. Yang, L. Xu, W. Li, W. Fan, S. Song, J. Yang, Adsorption and degradation of sulfadiazine over nanoscale zero-valent iron encapsulated in three-dimensional graphene network through oxygen-driven heterogeneous Fenton-like reactions, Appl. Catal. B Environ. 259 (2019) 118057, https://doi.org/10.1016/j.apcatb.2019.118057.
[59] J. Fan, H. Qin, Y. Zhang, S. Jiang, Degradation of 4-chlorophenol by BM Fe/Cu-O_2 system: the symbiosis of $\bullet O_2^-$ and •OH radicals, Water Environ. Res. 91 (8) (2019) 770–779, https://doi.org/10.1002/wer.1107.
[60] G. Dong, Z. Ai, L. Zhang, Total aerobic destruction of azo contaminants with nanoscale zero-valent copper at neutral pH: promotion effect of in-situ generated carbon center radicals, Water Res. 66 (2014) 22–30, https://doi.org/10.1016/j.watres.2014.08.011.
[61] R. Hong, Z. Guo, J. Gao, C. Gu, Rapid degradation of atrazine by hydroxyl radical induced from montmorillonite templated subnano-sized zero-valent copper, Chemosphere 180 (2017) 335–342, https://doi.org/10.1016/j.chemosphere.2017.04.025.
[62] Z. Yang, Y. Liu, J. Wang, MOF-derived Cu0/C activation of molecular oxygen for efficient degradation of sulfamethazine, Chem. Eng. J. 427 (2022) 131961, https://doi.org/10.1016/j.cej.2021.131961.
[63] J. Zhang, Y. Wu, L. Liu, Y. Lan, Rapid removal of p-chloronitrobenzene from aqueous solution by a combination of ozone with zero-valent zinc, Sep. Purif. Technol. 151 (2015) 318–323, https://doi.org/10.1016/j.seppur.2015.07.060.
[64] M. Ghasemi, A. Khataee, P. Gholami, R.D.C. Soltani, A. Hassani, Y. Orooji, In-situ electro-generation and activation of hydrogen peroxide using a CuFeNLDH-CNTs modified graphite cathode for degradation of cefazolin, J. Environ. Manag. 267 (2020) 110629, https://doi.org/10.1016/j.jenvman.2020.110629.
[65] A.I. Zárate-Guzmán, L.V. González-Gutiérrez, L.A. Godínez, A. Medel-Reyes, F. Carrasco-Marín, L.A. Romero-Cano, Towards understanding of heterogeneous Fenton reaction using carbon-Fe catalysts coupled to in-situ H_2O_2 electro-generation as clean technology for wastewater treatment, Chemosphere 224 (2019) 698–706, https://doi.org/10.1016/j.chemosphere.2019.02.101.
[66] X.-b. Gong, Z. Yang, L. Peng, A.-l. Zhou, Y.-l. Liu, Y. Liu, In-situ synthesis of hydrogen peroxide in a novel Zn-CNTs-O_2 system, J. Power Sources 378 (2018) 190–197, https://doi.org/10.1016/j.jpowsour.2017.12.040.
[67] Y. Liu, N. Tan, B. Wang, Y. Liu, Stepwise adsorption-oxidation removal of oxytetracycline by Zn^0-CNTs-Fe_3O_4 from aqueous solution, Chem. Eng. J. 375 (2019) 121963, https://doi.org/10.1016/j.cej.2019.121963.
[68] Y. Liu, Q. Fan, J. Wang, Zn-Fe-CNTs catalytic in situ generation of H_2O_2 for Fenton-like degradation of sulfamethoxazole, J. Hazard Mater. 342 (2018) 166–176, https://doi.org/10.1016/j.jhazmat.2017.08.016.
[69] Z. Yang, Y. Luo, J. Yue, X. Wang, H. Xu, Q. Ye, Y. Zhang, X. Xing, Q. Wang, J. Zhang, Activation of O_2 by zero-valent zinc assisted with Cu(II) for organics removal: performance and mechanism, J. Hazard Mater. 424 (2022) 127506, https://doi.org/10.1016/j.jhazmat.2021.127506.
[70] M. Foroughi, S.J. Peighambardoust, B. Ramavandi, D.C. Boffito, Simultaneous anionic dyes degradation via H_2O_2 activation using Zeolite 4A/ZnO/$Fe_2(MoO_4)_3$ nanoparticles in a sono-photocatalytic process, Adv. Polym. Technol. 35 (1) (2024), https://doi.org/10.1016/j.apt.2023.104320.
[71] X. Hou, W. Shen, X. Huang, Z. Ai, L. Zhang, Ascorbic acid enhanced activation of oxygen by ferrous iron: a case of aerobic degradation of rhodamine B, J. Hazard Mater. 308 (2016) 67–74, https://doi.org/10.1016/j.jhazmat.2016.01.031.
[72] Y. Zong, Y. Mao, L. Xu, D. Wu, Non-selective degradation of organic pollutants via dioxygen activation induced by Fe(II)-tetrapolyphosphate complexes: identification of reactive oxidant and kinetic modeling, Chem. Eng. J. 398 (2020) 125603, https://doi.org/10.1016/j.cej.2020.125603.
[73] H. Wang, L. Zhang, C. Hu, X. Wang, Enhanced Fenton-like catalytic performance of Cu-Al/KIT-6 and the key role of O_2 in triggering reaction, Chem. Eng. J. 387 (2020) 124006, https://doi.org/10.1016/j.cej.2019.124006.
[74] N. Zheng, X. He, Q. Zhou, R. Wang, X. Zhang, R. Hu, Z. Hu, Generation of reactive chlorine species via molecular oxygen activation on a copper chloride loaded hydrothermal carbonaceous carbon for advanced oxidation process, Appl. Catal. B Environ. 319 (2022) 121918, https://doi.org/10.1016/j.apcatb.2022.121918.
[75] N. Zheng, L. Li, X. Tang, W. Xie, Q. Zhu, X. Wang, Y. Lian, J.C. Yu, Z. Hu, Spontaneous formation of low valence copper on red phosphorus to effectively activate molecular oxygen for advanced oxidation process, Environ. Sci. Technol. 57 (12) (2023) 5024–5033, https://doi.org/10.1021/acs.est.2c09645.
[76] N. Zheng, X. Tang, Y. Lian, Z. Ou, Q. Zhou, R. Wang, Z. Hu, Low-valent copper on molybdenum triggers molecular oxygen activation to selectively generate singlet oxygen for advanced oxidation processes, J. Hazard Mater. 452 (2023) 131210, https://doi.org/10.1016/j.jhazmat.2023.131210.
[77] C. Zhang, C. Kong, P.G. Tratnyek, C. Qin, Y. Zhao, Y. Piao, Effect of interfacial action on the generation and transformation of reactive oxygen species in

tripolyphosphate-enhanced heterogeneous Fe_3O_4/O_2 systems, Environ. Sci. Technol. 58 (2024) 1378–1389, https://doi.org/10.1021/acs.est.3c07372.
[78] Z. Hu, Z. Wu, C. Han, J. He, Z. Ni, W. Chen, Two-dimensional transition metal dichalcogenides: interface and defect engineering, Chem. Soc. Rev. 47 (9) (2018) 3100–3128, https://doi.org/10.1039/C8CS00024G.
[79] L. Wu, Z. Sun, Y. Zhen, S. Zhu, C. Yang, J. Lu, Y. Tian, D. Zhong, J. Ma, Oxygen vacancy-induced nonradical degradation of organics: critical trigger of oxygen (O_2) in the Fe-Co LDH/Peroxymonosulfate system, Environ. Sci. Technol. 55 (22) (2021) 15400–15411, https://doi.org/10.1021/acs.est.1c04600.
[80] S. Wang, J. Zhu, T. Li, F. Ge, Z. Zhang, R. Zhu, H. Xie, Y. Xu, Oxygen vacancy-mediated CuCoFe/Tartrate-LDH catalyst directly activates oxygen to produce superoxide radicals: transformation of active species and implication for nitrobenzene degradation, Environ. Sci. Technol. 56 (12) (2022) 7924–7934, https://doi.org/10.1021/acs.est.2c00522.
[81] S. Wang, T. Li, X. Cheng, R. Zhu, Y. Xu, Regulating the concentration of dissolved oxygen to achieve the directional transformation of reactive oxygen species: a controllable oxidation process for ciprofloxacin degradation by calcined CuCoFe-LDH, Water Res. 233 (2023) 119744, https://doi.org/10.1016/j.watres.2023.119744.
[82] Y.J. Hao, B. Liu, L.G. Tian, F.T. Li, J. Ren, S.J. Liu, Y. Liu, J. Zhao, X.J. Wang, Synthesis of 111 Facet-exposed MgO with surface oxygen vacancies for reactive oxygen species generation in the dark, ACS Appl. Mater. Interfaces 9 (14) (2017) 12687–12693, https://doi.org/10.1021/acsami.6b16856.
[83] V. Lakshmi Prasanna, R. Vijayaraghavan, Insight into the mechanism of antibacterial activity of ZnO: surface defects mediated reactive oxygen species even in the dark, Langmuir 31 (33) (2015) 9155–9162, https://doi.org/10.1021/acs.langmuir.5b02266.
[84] W.T. Yein, Q. Wang, Y. Liu, Y. Li, J. Jian, X. Wu, Piezo-potential induced molecular oxygen activation of defect-rich MoS_2 ultrathin nanosheets for organic dye degradation in dark, J. Environ. Chem. Eng. 8 (1) (2020) 103626, https://doi.org/10.1016/j.jece.2019.103626.
[85] J. Ji, Q. Yan, P. Yin, S. Mine, M. Matsuoka, M. Xing, Defects on CoS_{2-x}: tuning redox reactions for sustainable degradation of organic pollutants, Angew. Chem., Int. Ed. Engl. 60 (6) (2021) 2903–2908, https://doi.org/10.1002/ange.202013015.
[86] J. Liu, Z. Yao, G. Qiu, Y. Wan, W. Song, H. Zeng, F. Yang, D. Zhao, W. Yuan, P. Ju, R. Lin, H. Zhou, L. Shi, K. Hu, Generation of reactive oxygen species through dissolved oxygen activation on defected porous carbon for efficient degradation of antibiotics, Chem. Eng. J. 455 (2023) 140602, https://doi.org/10.1016/j.cej.2022.140602.
[87] H. Zhao, L. Qian, Y. Chen, Q. Wang, G. Zhao, Selective catalytic two-electron O_2 reduction for onsite efficient oxidation reaction in heterogeneous electro-Fenton process, Chem. Eng. J. 332 (2018) 486–498, https://doi.org/10.1016/j.cej.2017.09.093.
[88] H. Xu, H. Guo, C. Chai, N. Li, X. Lin, W. Xu, Anodized graphite felt as an efficient cathode for in-situ hydrogen peroxide production and electro-Fenton degradation of rhodamine B, Chemosphere 286 (2022) 131936, https://doi.org/10.1016/j.chemosphere.2021.131936.
[89] Y. Xu, Z. Mao, R. Qu, J. Wang, J. Yu, X. Luo, M. Shi, X. Mao, J. Ding, B. Liu, Electrochemical hydrogenation of oxidized contaminants for water purification without supporting electrolyte, Nat. Water 1 (1) (2023) 95–103, https://doi.org/10.1038/s44221-022-00002-3.
[90] X. Shen, F. Xiao, H. Zhao, Y. Chen, C. Fang, R. Xiao, W. Chu, G. Zhao, In situ-formed PdFe nanoalloy and carbon defects in cathode for synergic reduction–oxidation of chlorinated pollutants in electro-Fenton process, Environ. Sci. Technol. 54 (7) (2020) 4564–4572. https://pubs.acs.org/doi/10.1021/acs.est.9b05896.
[91] L. Jin, M. Liu, S. You, H. Zhao, Y. Liu, Electrocatalytic membrane with p-block bismuth atoms for selective oxygen activation to hydroxyl radicals for effective water decontamination, Appl. Catal. B Environ. 352 (2024) 124044, https://doi.org/10.1016/j.apcatb.2024.124044.
[92] Y. Wang, J. Chen, J. Gao, H. Meng, S. Chai, Y. Jian, L. Shi, Y. Wang, C. He, Selective electrochemical H_2O_2 generation on the graphene aerogel for efficient electro-Fenton degradation of ciprofloxacin, Sep. Purif. Technol. 272 (2021) 118884, https://doi.org/10.1016/j.seppur.2021.118884.
[93] J. Gu, J. Xie, S. Li, G. Song, M. Zhou, Highly efficient electro-peroxone enhanced by oxygen-doped carbon nanotubes with triple role of in-situ H_2O_2 generation, activation and catalytic ozonation, Chem. Eng. J. 452 (2023) 139597, https://doi.org/10.1016/j.cej.2022.139597.
[94] L. Jin, X. Duan, M. Sun, C.D. Vecitis, H. Yu, Y. Liu, A general strategy to synthesize fluidic single atom electrodes for selective reactive oxygen species production, ACS Nano 17 (13) (2023) 12875–12883. https://pubs.acs.org/doi/10.1021/acsnano.3c04521.
[95] L. Yang, D. Xu, X. Luo, X. Zhu, J. Zhao, J. Song, Y. Han, G. Li, X. Gao, L. Liu, Fe (II)-modulated microporous electrocatalytic membranes for organic micro-contaminant oxidation and fouling control: mechanisms of regulating electron transport toward enhanced reactive oxygen species activation, Environ. Sci. Technol. 57 (47) (2023) 19000–19011. https://pubs.acs.org/doi/10.1021/acs.est.3c01792.
[96] Z. Feng, M. Chen, Q. Yang, Z. Wang, L. Li, H. Zhao, G. Zhao, New insights into selective singlet oxygen production via the typical electroactivation of oxygen for water decontamination, Environ. Sci. Technol. 57 (44) (2023) 17123–17131. https://pubs.acs.org/doi/10.1021/acs.est.3c06336.
[97] N. Yan, T. Ren, K. Lu, Y. Gao, M. Sun, X. Huang, X. Zhang, Carbon-based electrocatalytic dual-membrane system bolsters singlet oxygen production for ultrafast water decontamination, J. Hazard Mater. 463 (2024) 132787, https://doi.org/10.1016/j.jhazmat.2023.132787.
[98] X. Bai, Y. Li, L. Xie, X. Liu, S. Zhan, W. Hu, A novel Fe-free photo-electro-Fenton-like system for enhanced ciprofloxacin degradation: bifunctional Z-scheme WO_3/gC_3N_4, Environ. Sci.: Nano 6 (9) (2019) 2850–2862, https://doi.org/10.1039/C9EN00528E.
[99] K. Wang, Z. Mo, S. Tang, M. Li, H. Yang, B. Long, Y. Wang, S. Song, Y. Tong, Photo-enhanced Zn–air batteries with simultaneous highly efficient in situ H_2O_2 generation for wastewater treatment, J. Mater. Chem. A 7 (23) (2019) 14129–14135, https://doi.org/10.1039/C9TA04253A.
[100] X. Du, P. Su, W. Fu, Q. Zhang, M. Zhou, Heterogeneous photoelectro-Fenton catalyzed by FeCu@PC for efficient degradation of sulfamethazine, Electrochim. Acta 412 (2022) 140122, https://doi.org/10.1016/j.electacta.2022.140122.
[101] Z. Ye, D.R.V. Guelfi, G. Álvarez, F. Alcaide, E. Brillas, I. Sirés, Enhanced electrocatalytic production of H_2O_2 at Co-based air-diffusion cathodes for the photoelectro-Fenton treatment of bronopol, Appl. Catal. B Environ. 247 (2019) 191–199, https://doi.org/10.1016/j.apcatb.2019.01.029.
[102] A.C.N. Pinheiro, T.S. Bernardino, F.E.B. Junior, M.R.V. Lanza, W.R.P. Barros, Enhanced electrodegradation of the Sunset Yellow dye in acid media by heterogeneous photoelectro-Fenton process using Fe_3O_4 nanoparticles as a catalyst, J. Environ. Chem. Eng. 8 (1) (2020) 103621, https://doi.org/10.1016/j.jece.2019.103621.
[103] I. Salmerón, K.V. Plakas, I. Sirés, I. Oller, M.I. Maldonado, A.J. Karabelas, S. Malato, Optimization of electrocatalytic H_2O_2 production at pilot plant scale for solar-assisted water treatment, Appl. Catal. B Environ. 242 (2019) 327–336, ttps://doi.org/10.1016/j.apcatb.2018.09.045.
[104] T.L. Yusuf, B.O. Orimolade, D. Masekela, B. Mamba, N. Mabuba, The application of photoelectrocatalysis in the degradation of rhodamine B in aqueous solutions: a review, RSC Adv. 12 (40) (2022) 26176–26191, https://doi.org/10.1039/D2RA04236C.
[105] H. Yu, Y. Xue, Y. Lu, X. Wang, S. Zhu, W. Qin, M. Huo, Novel application of a Z-scheme photocatalyst of Ag_3PO_4@g-C_3N_4 for photocatalytic fuel cells, J. Environ. Manag. 254 (2020) 109738, https://doi.org/10.1016/j.jenvman.2019.109738.
[106] M.G. Peleyeju, O.A. Arotiba, Recent trend in visible-light photoelectrocatalytic systems for degradation of organic contaminants in water/wastewater, Environ Sci-Wat Res 4 (10) (2018) 1389–1411, https://doi.org/10.1039/C8EW00276B.
[107] F. Ye, T. Wang, X. Quan, H. Yu, S. Chen, Constructing efficient WO_3-FPC system for photoelectrochemical H_2O_2 production and organic pollutants degradation, Chem. Eng. J. 389 (2020) 123427, https://doi.org/10.1016/j.cej.2019.123427.
[108] R. Kaushik, K. Sharma, P. Felix Siril, A. Halder, Design and investigation of photoelectrochemical water treatment using self-standing $Fe_3O_4/NiCO_2O_4$ photoanode: in-situ H_2O_2 generation and fenton-like activation, Chem. Eng. J. 479 (2024) 147575, https://doi.org/10.1016/j.cej.2023.147575.
[109] Y. Sun, L. Han, P. Strasser, A comparative perspective of electrochemical and photochemical approaches for catalytic H_2O_2 production, Chem. Soc. Rev. 49 (18) (2020) 6605–6631, https://doi.org/10.1039/D0CS00458H.
[110] A. Singh, S.K. Sarma, S. Karmakar, S. Basu, Photocatalytic H_2O_2 generation assisted photoelectrochemical water oxidation for enhanced $BiVO_4$ photoanode performance, CEJ advances 8 (2021) 100142, https://doi.org/10.1016/j.ceja.2021.100142.
[111] R. Liang, H. Wu, Z. Hu, J. Sun, C. Fu, S. Li, X. Zhang, M. Zhou, Novel photoelectrocatalytic system of oxygen vacancy-rich black TiO_{2-x} nanocones photoanode and natural air diffusion cathode for efficient water purification and simultaneous H_2O_2 production, Appl. Catal. B Environ. 352 (2024) 124042, https://doi.org/10.1016/j.apcatb.2024.124042.
[112] B. Zhang, X. Li, Y. Ma, T. Jiang, Y. Zhu, H. Ren, Visible-light photoelectrocatalysis/H_2O_2 synergistic degradation of organic pollutants by a magnetic Fe_3O_4@SiO_2@ mesoporous TiO_2 catalyst-loaded photoelectrode, RSC Adv. 12 (47) (2022) 30577–30587, https://doi.org/10.1039/D2RA05183D.
[113] Q. Dang, W. Zhang, J. Liu, L. Wang, D. Wu, D. Wang, Z. Lei, L. Tang, Bias-free driven ion assisted photoelectrochemical system for sustainable wastewater treatment, Nat. Commun. 14 (1) (2023) 8413, https://doi.org/10.1038/s41467-023-44155-5.
[114] Q. Chen, J. Li, X. Li, K. Huang, B. Zhou, W. Shangguan, Self-biasing photoelectrochemical cell for spontaneous overall water splitting under visible-light illumination, ChemSusChem 6 (7) (2013) 1276–1281, https://doi.org/10.1002/cssc.201200936.
[115] T.H. Jeon, B. Kim, C. Kim, C. Xia, H. Wang, P.J.J. Alvarez, W. Choi, Solar photoelectrochemical synthesis of electrolyte-free H_2O_2 aqueous solution without needing electrical bias and H_2, Energy Environ. Sci. 14 (5) (2021) 3110–3119, https://doi.org/10.1039/D0EE03567J.
[116] C. Dong, Y. Yang, X. Hu, Y. Cho, G. Jang, Y. Ao, L. Wang, J. Shen, J.H. Park, K. Zhang, Self-cycled photo-Fenton-like system based on an artificial leaf with a solar-to-H_2O_2 conversion efficiency of 1.46, Nat. Commun. 13 (1) (2022) 4982, https://doi.org/10.1038/s41467-022-32410-0.
[117] M. Sharma, M. Jalalah, S.A. Alsareii, F.A. Harraz, W. Xue, N. Thakur, E.-S. Salama, X. Li, Microalgal cycling in the cathode of microbial fuel cells (MFCs) induced oxygen reduction reaction (ORR) and electricity: a biocatalytic process for clean energy, Chem. Eng. J. 479 (2024) 147431, https://doi.org/10.1016/j.cej.2023.147431.

[118] D. Wang, J. Hu, B. Liu, H. Hou, J. Yang, Y. Li, Y. Zhu, S. liang, K. Xiao, Degradation of refractory organics in dual-cathode electro-Fenton using air-cathode for H_2O_2 electrogeneration and microbial fuel cell cathode for Fe^{2+} regeneration, J. Hazard Mater. 412 (2021) 125269, https://doi.org/10.1016/j.jhazmat.2021.125269.
[119] S. Bhaduri, M. Behera, From single-chamber to multi-anodic microbial fuel cells: a review, J. Environ. Manag. 355 (2024) 120465, https://doi.org/10.1016/j.jenvman.2024.120465.
[120] B.E. Logan, B. Hamelers, R. Rozendal, U. Schröder, J. Keller, S. Freguia, P. Aelterman, W. Verstraete, K. Rabaey, Microbial fuel cells: methodology and technology, Environ. Sci. Technol. 40 (17) (2006) 5181–5192. https://pubs.acs.org/doi/abs/10.1021/es0605016.
[121] X.-Y. Yong, D.-Y. Gu, Y.-D. Wu, Z.-Y. Yan, J. Zhou, X.-Y. Wu, P. Wei, H.-H. Jia, T. Zheng, Y.-C. Yong, Bio-electron-Fenton (BEF) process driven by microbial fuel cells for triphenyltin chloride (TPTC) degradation, J. Hazard Mater. 324 (2017) 178–183, https://doi.org/10.1016/j.jhazmat.2016.10.047.
[122] F. Soltani, N. Navidjouy, H. Khorsandi, M. Rahimnejad, S. Alizadeh, A novel bio-electro-Fenton system with dual application for the catalytic degradation of tetracycline antibiotic in wastewater and bioelectricity generation, RSC Adv. 11 (44) (2021) 27160–27173, https://doi.org/10.1039/d1ra04584a.
[123] W. Wang, Y. Lu, H. Luo, G. Liu, R. Zhang, S. Jin, A microbial electro-fenton cell for removing carbamazepine in wastewater with electricity output, Water Res. 139 (2018) 58–65, https://doi.org/10.1016/j.watres.2018.03.066.
[124] S. Rafaqat, F. Arshad, R. Shahid, N. Ali, Employing the cost-effective composite cathodes for bio-Fenton facilitated degradation of acid red 114 integrated into hydrogen peroxide synthesizing microbial fuel cell, Electrochim. Acta 487 (2024) 144141, https://doi.org/10.1016/j.electacta.2024.144141.
[125] S. Xue, Y. Zhang, T. Marhaba, W. Zhang, Aeration and dissolution behavior of oxygen nanobubbles in water, J. Colloid Interface Sci. 609 (2022) 584–591, https://doi.org/10.1016/j.jcis.2021.11.061.
[126] L. Wang, J. Ali, Z. Wang, N.A. Oladoja, R. Cheng, C. Zhang, G. Mailhot, G. Pan, Oxygen nanobubbles enhanced photodegradation of oxytetracycline under visible light: synergistic effect and mechanism, Chem. Eng. J. 388 (2020) 124227, https://doi.org/10.1016/j.cej.2020.124227.
[127] B. Wang, L. Wang, W. Cen, T. Lyu, P. Jarvis, Y. Zhang, Y. Zhang, Y. Han, L. Wang, G. Pan, K. Zhang, W. Fan, Exploring a chemical input free advanced oxidation process based on nanobubble technology to treat organic micropollutants, Environ. Pollut. 340 (Pt 1) (2024) 122877, https://doi.org/10.1016/j.envpol.2023.122877.
[128] A. Ghadimkhani, W. Zhang, T. Marhaba, Ceramic membrane defouling (cleaning) by air nano bubbles, Chemosphere 146 (2016) 379–384, https://doi.org/10.1016/j.chemosphere.2015.12.023.
[129] M. Panizza, M.A. Oturan, Degradation of Alizarin Red by electro-Fenton process using a graphite-felt cathode, Electrochim. Acta 56 (20) (2011) 7084–7087, https://doi.org/10.1016/j.electacta.2011.05.105.
[130] E. Petrucci, A. Da Pozzo, L. Di Palma, On the ability to electrogenerate hydrogen peroxide and to regenerate ferrous ions of three selected carbon-based cathodes for electro-Fenton processes, Chem. Eng. J. 283 (2016) 750–758, https://doi.org/10.1016/j.cej.2015.08.030.
[131] M. Liu, Z. Xing, H. Zhao, S. Song, Y. Wang, Z. Li, W. Zhou, An efficient photo-Fenton system for in-situ evolution of H_2O_2 via defective iron-based metal organic framework@$ZnIn_2S_4$ core-shell Z-scheme heterojunction nanoreactor, J. Hazard Mater. 437 (2022) 129436, https://doi.org/10.1016/j.jhazmat.2022.129436.
[132] W. Yang, K. Sun, J. Wan, Y.-A. Ma, J. Liu, B. Zhu, L. Liu, F. Fu, Boosting holes generation and O_2 activation by bifunctional NiCoP modified $Bi_4O_5Br_2$ for efficient photocatalytic aerobic oxidation, Appl. Catal. B Environ. 320 (2023) 121978, https://doi.org/10.1016/j.apcatb.2022.121978.
[133] Y. Nosaka, A.Y. Nosaka, Generation and detection of reactive oxygen species in photocatalysis, Chem. Rev. 117 (17) (2017) 11302–11336, https://doi.org/10.1021/acs.chemrev.7b00161.
[134] Q. Li, F.T. Li, Recent advances in molecular oxygen activation via photocatalysis and its application in oxidation reactions, Chem. Eng. J. 421 (2021) 129915, https://doi.org/10.1016/j.cej.2021.129915.
[135] J. Di, J. Xia, M. Ji, B. Wang, X. Li, Q. Zhang, Z. Chen, H. Li, Nitrogen-doped carbon quantum dots/BiOBr ultrathin nanosheets: in situ strong coupling and improved molecular oxygen activation ability under visible light irradiation, ACS Sustainable Chem. Eng. 4 (1) (2016) 136–146. https://doi/10.1021/acssuschemeng.5b00862.
[136] Y.-F. Liou, L.W. Wei, C. Chen, S.H. Liu, Y.C. Pu, H.P. Wang, Photocatalytic splitting of H_2O-to-H_2O_2 by BiOI/g-C_3N_4/CoP S-scheme heterojunctions, New J. Chem. 47 (4) (2023) 1825–1831, https://doi.org/10.1039/D2NJ04216A.
[137] Y. Wang, Y. Lin, S. He, S. Wu, C. Yang, Singlet oxygen: properties, generation, detection, and environmental applications, J. Hazard Mater. 461 (2024) 132538, https://doi.org/10.1016/j.jhazmat.2023.132538.
[138] M.P. Rayaroth, U.K. Aravind, G. Boczkaj, C.T. Aravindakumar, Singlet oxygen in the removal of organic pollutants: an updated review on the degradation pathways based on mass spectrometry and DFT calculations, Chemosphere 345 (2023) 140203, https://doi.org/10.1016/j.chemosphere.2023.140203.
[139] M.C. DeRosa, R.J. Crutchley, Photosensitized singlet oxygen and its applications, Coord. Chem. Rev. 233 (2002) 351–371, https://doi.org/10.1016/S0010-8545(02)00034-6.
[140] D.R. Kearns, Physical and chemical properties of singlet molecular oxygen, Chem. Rev. 71 (4) (1971) 395–427, https://doi.org/10.1021/cr60272a004.
[141] J. Chakraborty, I. Nath, F. Verpoort, A physicochemical introspection of porous organic polymer photocatalysts for wastewater treatment, Chem. Soc. Rev. 51 (3) (2022) 1124–1138, https://doi.org/10.1039/D1CS00916H.